An energy-consistent discretization of hyper-viscoelastic contact models for soft tissues

Mikaël Barboteu, Francesco Bonaldi, Serge Dumont, Christina Mahmoud

An energy-consistent discretization of hyper-viscoelastic contact models for soft tissues

Mikaël Barboteu*, Francesco Bonaldi*[1], Serge Dumont*, and Christina Mahmoud#

barboteu@univ-perp.fr, francesco.bonaldi@univ-perp.fr, serge.dumont@univ-perp.fr, christina.mahmoud@umontpellier.fr

*Laboratoire de Modélisation Pluridisciplinaire et Simulations
Université de Perpignan Via Domitia
52 Avenue Paul Alduy, 66860 Perpignan, France

#IMAG, Univ. Montpellier, CNRS, Montpellier, France

Abstract

In this work, we propose a mathematical model of hyper-viscoelastic problems applied to soft biological tissues, along with an energy-consistent numerical approximation. We first present the general problem in a dynamic regime, with certain types of dissipative constitutive assumptions. We then provide a numerical approximation of this problem, with the main objective of respecting energy consistency during contact in adequacy with the continuous framework. Given the presence of friction or viscosity, a dissipation of mechanical energy is expected. Moreover, we are interested in the numerical simulation of the non-smooth and non-linear problem considered, and more particularly in the optimization of Newton's semi-smooth method and Primal Dual Active Set (PDAS) approaches. Finally, we test such numerical schemes on academic and real-life scenarios, the latter representing the contact deployment of a stainless-steel stent in an arterial tissue.

AMS Subject Classification : 74M15, 74M20, 74M10, 74B20, 74H15, 74S30, 49M15, 90C53, 70F40, 70-08, 70E55, 35Q70

Keywords: Hyperelasticity, Unilateral Contact, Viscosity, Coulomb Friction, Energy consistency, Semi-Smooth Newton method, Primal-Dual Active Set, Numerical simulations, Biological soft tissues.

1. Introduction

Soft biological tissues, such as skin, tendons, or ligaments, play a primary role in the mechanical integrity of the human body. They are mainly made up of collagen and elastin proteins, which result in specific mechanical properties at the macroscopic scale. They can be stretched up to 15% without damage, and their behavior is also characterized by a significant viscous component.

Soft tissue biomechanical properties derived from experimental measurements [1] are critical for developing real-life-based models for minimally invasive surgical simulation (e.g., contact deployment of a stainless-steel stent

[1]Corresponding author.

in an arterial tissue [2]). The theory of elastic bodies subjected to large deformations has often been employed to model the physical behavior of biological tissues [3, 1, 4, 5]. Most phenomenological models are based on a non-linear elastic (*hyperelastic*) constitutive assumption for the material behavior [2, 6], in the light of the data obtained by experiments. In addition, most medical device regulators insist today on analyzing numerical simulations as part of their approval process.

The goal of this work is to study a hyperelastic dynamic model including viscosity. Hyperelastodynamic problems with contact and friction conditions lead to the study of impact and deformation of a hyperelastic body interacting with a foundation, and arise from non-smooth and non-linear constitutive laws. Such laws are quite challenging to deal with, both from a mathematical and a numerical perspective [7, 8, 9, 10, 11, 12, 13]. The dynamics can thus no longer be simulated by decomposition on the eigenmodes of the structure, which is standard in linear elastodynamics, and particular attention must be devoted to the choice of time integration schemes, very sensitive in terms of stability to the non-linearities of the physics. Indeed, energy consistency represents for time integration schemes a guarantee of numerical stability during the resolution of non-linear elastodynamic problems. Moreover, ensuring energy conservation in the case of impact problems is a key challenge. Many works have been carried out in order to determine numerical strategies specifically adapted to non-linear dynamics problems [14, 15, 16, 12, 13, 17].

First of all, time integration of non-linear elastodynamics equations is hindered by several difficulties [7, 14, 16, 13]. One is typically led to considering totally implicit schemes, but still, due to non-linearity, their stability remains a major issue [9]. Indeed, when the time step is not small enough, most schemes issued from the linear framework give rise to a blow-up of the total energy of the discrete system [7, 14]. This raises then the problem of energy conservation for time integrators, which represents a key stability criterion. Gonzalez proposed in [14] a numerical scheme complying with such a criterion. It is of particular interest in practice, since it provides an explicit expression of the stress terms appearing in the scheme. Furthermore, subsequent work demonstrates energy conservation methods for more general stored energy functions offering further insights for a broader class of materials [18, 19, 20, 21]. In order to obtain energy conservation properties for non-linear dynamic problems, it is necessary to take into account the persistence condition during impacts [22, 14, 15, 16, 13]. The persistence condition represents the complementarity condition of unilateral contact taken in this case between normal contact velocity and normal impulse force. Many references [16, 7, 23, 14, 24, 25, 26, 15, 13, 27, 28, 17] propose relevant approaches to solve such impact problems with energy balance properties. Several relevant references [29, 30, 31, 32, 33, 34, 35, 36] concerning energy-momentum approaches and geometric admissibility have made it possible to improve the algorithmic performance of such contact problems. Since several numerical approximations give rise to either artificial dissipations or increase in energy, we propose in this paper a model in adequacy with energy consistency of hyperelastic frictional contact systems, with an extension to viscosity [7, 13, 37, 19]. Several methods have been successfully tested to solve frictional contact problems. Some are based on treatment of contact conditions by normal compliance [38, 39, 40, 41] or by other relevant methods such as the quasi-augmented Lagrangian method [42], the bi-potential method [43, 44], the conjugate gradient method [7, 8], the Uzawa method [45, 46], and the Nitsche finite element method [47, 48, 49, 50]. Recently, Primal-Dual Active Set (PDAS) methods have emerged as promising in solving contact problems with friction in a deformable medium, due to their efficiency and ease of implementation [51, 52, 53, 54, 41]. From a purely algorithmic point of view, the main objective of these methods is to separate the nodes potentially in contact into two subsets (active and inactive) and to find the right subset of all the nodes actually in contact (subset $\mathcal{A}$) as opposed to those which are inactive (subset $\mathcal{I}$). In practice, these methods do not involve Lagrange multipliers (such as in the augmented quasi-Lagrangian method). In fact, the boundary conditions on subsets $\mathcal{A}$ and $\mathcal{I}$ are directly imposed thanks to a semi-smooth Newton method. Recall that these methods have been developed recently for unilateral contact conditions [51, 52, 53, 54, 55], and in particular in [56], supplemented by those in [57, 58].

This paper is organized into six sections. We present the physical framework and the mathematical model,

and recall the constitutive assumptions for hyper-viscoelastic materials in Section 2. We then give the strong and variational formulations of the problem by detailing the properties of energy conservation and dissipation in the continuous case using the persistence condition. Section 3 is devoted to the discretization of the hyper-viscoelastic problem with contact and the energy-consistent approach adapted to frictional contact. In Sections 4 and 5, we present the numerical simulation of the non-smooth and non-linear problems considered previously, focusing on the optimization of Newton's semi-smooth and PDAS methods. We then validate these PDAS schemes on benchmarks representing academic test cases carried out with a linear elastic ball and a hyperelastic ring, both launched in the direction of a rigid foundation. In the last section, we test such numerical approaches on a real-life application representing the contact deployment of a stainless-steel stent in an arterial tissue.

2. Mechanical and mathematical modeling

2.1. Mechanical Modeling

Dynamical systems of deformable bodies undergoing large deformations are governed by non-linear time-dependent equations. Let $d \in \{2,3\}$ denote the space dimension. In this work, we consider the referential configurations (open, bounded, and connected sets) $\Omega^{(1)} \subset \mathbb{R}^d$ and $\Omega^{(2)} \subset \mathbb{R}^d$ of two continuous bodies, each one characterized by a hyperelastic constitutive law. Let $i \in \{1,2\}$. The spatial configuration of deformable body $\Omega^{(i)}$ at time $t \in (0,T)$, denoted by $\Omega_t^{(i)}$, is defined by the deformation mapping $\boldsymbol{\varphi}^{(i)}$ as follows:

$$\begin{aligned} \boldsymbol{\varphi}^{(i)} : \Omega^{(i)} \times (0,T) &\to \Omega_t^{(i)} \subset \mathbb{R}^d, \\ (\mathbf{x}^{(i)}, t) &\mapsto \boldsymbol{\varphi}^{(i)}(\mathbf{x}^{(i)}, t) = \mathbf{x}^{(i)} + \mathbf{u}^{(i)}(\mathbf{x}^{(i)}, t), \end{aligned}$$

where $\mathbf{u}^{(i)}$ represents the displacement vector field relative to body $\Omega^{(i)}$. This mapping must be of class C^1 on $\overline{\Omega}^{(i)}$, invertible, and orientation-preserving. The first Piola–Kirchhoff tensor $\boldsymbol{\Pi}^{(i)}$ is given by $\boldsymbol{\Pi}^{(i)} = \partial_{\mathbf{F}} W^{(i)}(\mathbf{F}^{(i)})$, where $W^{(i)}(\mathbf{F}^{(i)})$ is the elastic energy density, and $\mathbf{F}^{(i)}$ the deformation gradient, such that $\mathbf{F}^{(i)} = \nabla \boldsymbol{\varphi}^{(i)} = \mathbf{I} + \nabla \mathbf{u}^{(i)}$. For more details about the hyperelastic framework, we refer to [59, 60]. Thereafter, $\square^{(i)}$ represents quantity $\square$ pertaining to $\Omega^{(i)} \cup \partial\Omega^{(i)}$. The subset $\partial_c\Omega^{(i)} \subset \partial\Omega^{(i)}$ is the contact surface of body $\Omega^{(i)}$ (see Figure 1) and we let $\partial_c\Omega \coloneqq \partial_c\Omega^{(1)} \cup \partial_c\Omega^{(2)}$.

To introduce contact and friction, we need the tangent plane of the current contact surface $\partial_c\Omega_t^{(2)}$ and its outer unit normal vector field, denoted by $\boldsymbol{\nu}$. The tangent plane of $\partial_c\Omega_t^{(2)}$ is $\mathcal{T}_{\boldsymbol{\varphi}^{(2)}} \coloneqq \left\{\mathbf{z} \in \mathbb{R}^d : \mathbf{z} \cdot \boldsymbol{\nu} = 0\right\}$. Frictional contact is modeled by combining the normal unilateral contact law and the tangential law of Coulomb's friction with variable pressure [7, 8, 61, 62, 63, 42, 50]. These relations depend on the normal distance $d_{\boldsymbol{\nu}}$, the tangential contact velocity $\overset{\circ}{\mathbf{d}}_{\boldsymbol{\tau}}$, and the contact and friction stress $\boldsymbol{\Gamma}$ (which is split into a normal contact stress $\Gamma_{\boldsymbol{\nu}}$ and a tangential stress $\boldsymbol{\Gamma}_{\boldsymbol{\tau}}$). These laws are the

$$\text{Contact law: } \begin{cases} d_{\boldsymbol{\nu}} \geq 0, \\ \Gamma_{\boldsymbol{\nu}} \leq 0, \\ d_{\boldsymbol{\nu}}\Gamma_{\boldsymbol{\nu}} = 0, \end{cases} \quad \text{and the Friction law: } \begin{cases} \overset{\circ}{\mathbf{d}}_{\boldsymbol{\tau}} = \|\overset{\circ}{\mathbf{d}}_{\boldsymbol{\tau}}\| \dfrac{\boldsymbol{\Gamma}_{\boldsymbol{\tau}}}{\|\boldsymbol{\Gamma}_{\boldsymbol{\tau}}\|}, \\ \|\boldsymbol{\Gamma}_{\boldsymbol{\tau}}\| + \mu\Gamma_{\boldsymbol{\nu}} \leq 0, \\ \|\overset{\circ}{\mathbf{d}}_{\boldsymbol{\tau}}\|(\|\boldsymbol{\Gamma}_{\boldsymbol{\tau}}\| + \mu\Gamma_{\boldsymbol{\nu}}) = 0, \end{cases} \quad \text{on} \quad \partial_c\Omega. \tag{2.1}$$

Here, $\|\cdot\|$ is the Euclidean norm, $\boldsymbol{\nu}$ and $\boldsymbol{\tau} \in \mathcal{T}_{\boldsymbol{\varphi}^{(2)}}$ are the unit normal and tangential vector fields on $\partial_c\Omega_t^{(2)}$, and $\mu \geq 0$ is the friction coefficient. The *normal* and *tangential distances* can be defined, for any $(\mathbf{x}^{(1)}, \mathbf{x}^{(2)}) \in \partial_c\Omega^{(1)} \times \partial_c\Omega^{(2)}$ and fixed $t > 0$, as follows. First, we introduce the projection of the nearest point $\mathbf{x}^{\perp(2)}$ (*proximal point*) on the target surface $\partial_c\Omega^{(2)}$ as

$$\mathbf{x}^{\perp(2)} \coloneqq \underset{\mathbf{x}^{(2)} \in \partial_c\Omega^{(2)}}{\operatorname{argmin}} \|(\mathbf{x}^{(1)} + \mathbf{u}^{(1)}(\mathbf{x}^{(1)}, t)) - (\mathbf{x}^{(2)} + \mathbf{u}^{(2)}(\mathbf{x}^{(2)}, t))\| \tag{2.2}$$

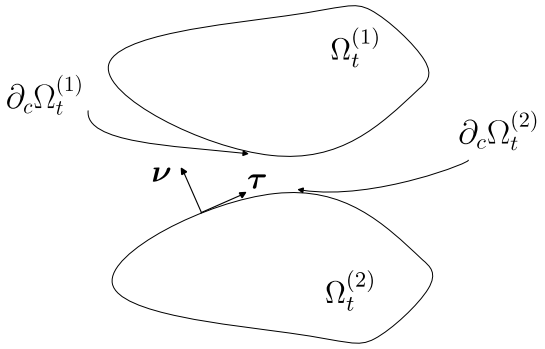

Figure 1: Physical setting of two deformable bodies $\Omega^{(i)}$ in contact, in a two-dimensional framework.

The necessary condition for the minimization problem (2.2) to admit a solution, i.e., for the distance separating $\mathbf{x}^{(1)} + \mathbf{u}^{(1)}(\mathbf{x}^{(1)}, t)$ from $\mathbf{x}^{(2)} + \mathbf{u}^{(2)}(\mathbf{x}^{(2)}, t)$ to be minimal, is the orthogonality condition

$$\Big[(\mathbf{x}^{(1)} + \mathbf{u}^{(1)}(\mathbf{x}^{(1)}, t)) - (\mathbf{x}^{(2)} + \mathbf{u}^{(2)}(\mathbf{x}^{(2)}, t))\Big] \cdot \mathrm{d}\boldsymbol{\varphi}^{(2)} = 0, \quad \forall \mathrm{d}\boldsymbol{\varphi}^{(2)} \in \mathcal{T}_{\boldsymbol{\varphi}^{\perp}}, \tag{2.3}$$

with $\mathcal{T}_{\boldsymbol{\varphi}^{\perp}}$ the tangent plane at the point $\boldsymbol{\varphi}^{\perp} = \boldsymbol{\varphi}^{(2)}(\mathbf{x}^{\perp}, t)$ defined as the point of $\partial_c\Omega_t^{(2)}$ closest to the point $\boldsymbol{\varphi}^{(1)}$ of $\partial_c\Omega_t^{(1)}$. Consequently, $\boldsymbol{\varphi}^{\perp}$ is the orthogonal projection of $\boldsymbol{\varphi}^{(1)}$ on $\partial_c\Omega_t^{(2)}$, and $\mathbf{x}^{\perp}$ is defined as the reciprocal image of this point $\boldsymbol{\varphi}^{\perp}$ by the application $\boldsymbol{\varphi}^{(2)}$:

$$\mathbf{x}^{\perp} = {\boldsymbol{\varphi}^{(2)}}^{-1}\left(\boldsymbol{\varphi}^{\perp}(\boldsymbol{\varphi}^{(1)}(\mathbf{x}^{(1)}, t), t), t\right). \tag{2.4}$$

Note that, because of large deformations, it is possible that the point $\boldsymbol{\varphi}^{\perp}(\boldsymbol{\varphi}^{(1)}(\mathbf{x}^{(1)}, t), t)$ not be defined. In this case, contact does not occur, and the relation (2.3) is no longer valid. Furthermore, we can notice that the uniqueness of the problem (2.2) is not always verified. The analysis of this remark is made in [64].
Then, the normal and tangential distances are defined, respectively, by:

$$d_{\boldsymbol{\nu}} \coloneqq \boldsymbol{\nu} \cdot \Big((\mathbf{x}^{(1)} + \mathbf{u}^{(1)}(\mathbf{x}^{(1)}, t)) - (\mathbf{x}^{\perp(2)} + \mathbf{u}^{(2)}(\mathbf{x}^{\perp(2)}, t))\Big), \tag{2.5}$$

$$\mathbf{d}_{\boldsymbol{\tau}} \coloneqq (\mathbf{I} - \boldsymbol{\nu} \otimes \boldsymbol{\nu}) \Big((\mathbf{x}^{(1)} + \mathbf{u}^{(1)}(\mathbf{x}^{(1)}, t)) - (\mathbf{x}^{\perp(2)} + \mathbf{u}^{(2)}(\mathbf{x}^{\perp(2)}, t))\Big), \tag{2.6}$$

where $\boldsymbol{\nu} = \boldsymbol{\nu}(\boldsymbol{\varphi}^{(2)}(\mathbf{x}^{(2)}, t), t)$. Similarly, we can define the normal and tangential contact velocities based on the velocities $\dot{\mathbf{u}}^{(i)}$:

$$\overset{\circ}{d}_{\boldsymbol{\nu}} \coloneqq \boldsymbol{\nu} \cdot (\dot{\mathbf{u}}^{(1)}(\mathbf{x}^{(1)}, t) - \dot{\mathbf{u}}^{(2)}(\mathbf{x}^{\perp(2)}, t)), \tag{2.7}$$

$$\overset{\circ}{\mathbf{d}}_{\boldsymbol{\tau}} \coloneqq (\mathbf{I} - \boldsymbol{\nu} \otimes \boldsymbol{\nu})(\dot{\mathbf{u}}^{(1)}(\mathbf{x}^{(1)}, t) - \dot{\mathbf{u}}^{(2)}(\mathbf{x}^{\perp(2)}, t)). \tag{2.8}$$

were the dot superscript denotes a time derivative. For more details on the definition of the quantities $d_{\boldsymbol{\nu}}$, $\overset{\circ}{d}_{\boldsymbol{\nu}}$ and $\mathbf{d}_{\boldsymbol{\tau}}$, $\overset{\circ}{\mathbf{d}}_{\boldsymbol{\tau}}$ in the context of large deformations, we refer the reader to [65, 7, 13, 17]. Moreover, in order to obtain energy conservation properties, the power of the normal contact reaction at time $t > 0$ must vanish [7, 61, 13]. Thus, to conserve energy, we add the *persistence condition* in the contact law:

$$\overset{\circ}{d}_{\boldsymbol{\nu}}\, \Gamma_{\boldsymbol{\nu}} = 0 \quad \text{on} \quad \partial_c\Omega_t. \tag{2.9}$$

This condition means that normal contact reactions are only active during persistent contact. One can easily prove (see [7, 8, 13]) that adding the persistence condition (2.9) to the law of unilateral contact in displacement (2.1) yields

the

$$\text{Persistent contact law:} \quad \begin{cases} \text{if } d_{\boldsymbol{\nu}} > 0 & \Gamma_{\boldsymbol{\nu}} = 0 \\ \text{if } d_{\boldsymbol{\nu}} = 0 & \overset{\circ}{d}_{\boldsymbol{\nu}} \geq 0,\ \Gamma_{\boldsymbol{\nu}} \leq 0,\ \overset{\circ}{d}_{\boldsymbol{\nu}}\, \Gamma_{\boldsymbol{\nu}} = 0 \end{cases} \quad \text{on} \quad \partial_c \Omega_t. \tag{2.10}$$

2.2. Mathematical modeling

2.2.1. Hyper-viscoelastic energy density

In this section, we extend the hyperelastic problem to viscosity. Therefore, we consider a stress tensor $\mathbf{\Pi}$ characterized by a Kelvin–Voigt law which allows to satisfy the fundamental requirement of infinitesimal framework indifference:

$$\mathbf{\Pi}(\mathbf{F}, \dot{\mathbf{F}}) = \frac{\partial W^e(\mathbf{F})}{\partial \mathbf{F}} + \frac{\partial W^v(\mathbf{F}, \dot{\mathbf{F}})}{\partial \dot{\mathbf{F}}}, \tag{2.11}$$

where W^e is the elastic energy density and W^v is the viscous power density. The function $\mathbf{\Pi}^e : \mathbb{M}^d \to \mathbb{M}^d$ is the hyperelastic operator (elastic part of stress), derived from the density W^e, such that

$$\mathbf{\Pi}^e(\mathbf{F}) = \frac{\partial W^e(\mathbf{F})}{\partial \mathbf{F}}, \tag{2.12}$$

and $\mathbf{\Pi}^v : \mathbb{M}^d \times \mathbb{M}^d \to \mathbb{M}^d$ is the viscosity operator (viscous part of stress), such that

$$\mathbf{\Pi}^v(\mathbf{F}, \dot{\mathbf{F}}) = \frac{\partial W^v(\mathbf{F}, \dot{\mathbf{F}})}{\partial \dot{\mathbf{F}}}. \tag{2.13}$$

The viscosity operator has to satisfy the Legendre–Hadamard (dissipation) condition, i.e. $\mathbf{\Pi}^v(\mathbf{F}, \dot{\mathbf{F}}) : \dot{\mathbf{F}} \geq 0$, $\forall \dot{\mathbf{F}} \in \mathbb{M}^d$. Let $\mathbf{C} = \mathbf{F}^T\mathbf{F}$ denote the right Cauchy–Green tensor. It is a simple matter to prove that this condition is satisfied, for instance, by the viscous power density proposed by Curnier [66], i.e.

$$W_1^v(\dot{\mathbf{C}}) = \frac{\eta}{2} \operatorname{tr}(\dot{\mathbf{C}}^2), \quad \eta > 0,$$

and by the one proposed by Pioletti *et al.* [67, 3], i.e.

$$W_2^v(\dot{\mathbf{C}}) = \frac{\eta}{4} \operatorname{tr}(\dot{\mathbf{C}}^2)(\operatorname{tr}(\mathbf{C}) - 3), \quad \eta > 0. \tag{2.14}$$

2.2.2. Strong formulation of the mechanical problem

We assume hereafter that a system of body forces $\mathbf{f} : \Omega^{(i)} \times (0,T) \to \mathbb{R}^d$ and surface forces $\mathbf{g} : \partial\Omega^{(i)} \times (0,T) \to \mathbb{R}^d$, for $i \in \{1,2\}$, is given. The strong formulation of the problem, involving the equations of motion of the hyper-viscoelastic body $\Omega^{(i)}$, for $i \in \{1,2\}$ without contact, is the following.

Problem $\mathcal{P}_S^{(i)}$. *Find the displacement field $\mathbf{u} : \Omega^{(i)} \times (0,T) \to \mathbb{R}^d$ and the stress field $\mathbf{\Pi} : \Omega^{(i)} \times (0,T) \to \mathbb{M}^d$ such that, for $i \in \{1,2\}$,*

$$\mathbf{\Pi}(\mathbf{F}, \dot{\mathbf{F}}) = \mathbf{\Pi}^e(\mathbf{F}) + \mathbf{\Pi}^v(\mathbf{F}, \dot{\mathbf{F}}) \quad \text{in} \quad \Omega^{(i)} \times (0,T), \tag{2.15}$$

$$\rho\ddot{\mathbf{u}} - \operatorname{Div} \mathbf{\Pi} = \mathbf{f} \quad \text{in} \quad \Omega^{(i)} \times (0,T), \tag{2.16}$$

$$\mathbf{u} = \mathbf{0} \quad \text{on} \quad \partial_0\Omega^{(i)} \times (0,T), \tag{2.17}$$

$$\mathbf{\Pi}\boldsymbol{\nu} = \mathbf{g} \quad \text{on} \quad \partial_g\Omega^{(i)} \times (0,T), \tag{2.18}$$

$$\mathbf{u}(0) = \mathbf{u}_0,\ \dot{\mathbf{u}}(0) = \mathbf{u}_1 \quad \text{in} \quad \Omega^{(i)}, \tag{2.19}$$

with $\mathbf{\Pi}^e(\mathbf{F}) = \partial_{\mathbf{F}} W^e(\mathbf{F})$ and $\mathbf{\Pi}^v(\mathbf{F}, \dot{\mathbf{F}}) = \partial_{\dot{\mathbf{F}}} W^v(\dot{\mathbf{F}})$. The subsets $\partial_0\Omega^{(i)}$ and $\partial_g\Omega^{(i)}$ of the boundary $\partial\Omega^{(i)}$ are, respectively, those on which displacement and traction are imposed. Equation (2.15) represents the hyper-viscoelastic constitutive law of the material, (2.16) represents the equation of motion in which ρ is the referential material density, and (2.17)–(2.18) are the boundary conditions for displacement and traction. Here, $\mathbf{f}$ and $\mathbf{g}$ always designate referential volume and surface forces, respectively. We denote by the same letter $\boldsymbol{\nu}$ both the current and referential outward normals to the boundary on which surface loads are imposed. Notice that $\mathbf{f}$ and $\mathbf{g}$ are not assumed to be dead loads, but they are just the referential counterparts of current loads that can, in principle, depend on the body motion. In the case of conservative volume and surface forces $\mathbf{f}(\mathbf{x}, t)$ and $\mathbf{g}(\mathbf{x}, t)$, the corresponding terms in the principle of virtual work can be expressed as Gateaux derivatives of force potentials:

$$DB(\boldsymbol{\varphi}; \mathbf{v}) = \nabla B(\boldsymbol{\varphi}) \cdot \mathbf{v} = \int_\Omega \mathbf{f}(\mathbf{x}, t) \cdot \mathbf{v}(\mathbf{x}) \, \mathrm{d}x, \tag{2.20}$$

$$DP(\boldsymbol{\varphi}; \mathbf{v}) = \nabla P(\boldsymbol{\varphi}) \cdot \mathbf{v} = \int_{\partial_g\Omega} \mathbf{g}(\mathbf{x}, t) \cdot \mathbf{v}(\mathbf{x}) \, \mathrm{d}a, \tag{2.21}$$

where $\mathbf{v}$ is in the space of kinematically admissible velocities satisfying boundary conditions on $\partial_0\Omega$, and $B(\boldsymbol{\varphi}; \cdot)$, $P(\boldsymbol{\varphi}, \cdot)$ denote the volume and surface potentials. When assuming in addition that applied forces are dead loads, i.e., independent of the deformation $\boldsymbol{\varphi}(\mathbf{x}, t)$, then the potentials $B(\boldsymbol{\varphi})$, $P(\boldsymbol{\varphi})$ can be expressed as

$$B(\boldsymbol{\varphi}) = \int_\Omega \mathbf{f}(\mathbf{x}) \cdot \boldsymbol{\varphi}(\mathbf{x}, t) \, \mathrm{d}x,$$
$$P(\boldsymbol{\varphi}) = \int_{\partial_g\Omega} \mathbf{g}(\mathbf{x}) \cdot \boldsymbol{\varphi}(\mathbf{x}, t) \, \mathrm{d}a.$$

The strong formulation of the problem for the system of hyper-viscoelastic bodies $\Omega = \Omega^{(1)} \cup \Omega^{(2)}$ with Coulomb frictional combined with persistence condition is obtained from the above problem by replacing $\Omega^{(i)}$ by Ω in each of Equations (2.15)–(2.19), and adding the corresponding contact conditions.

Problem $\mathcal{P}_S^c$. *Find the displacement field* $\mathbf{u} : \Omega \times (0, T) \to \mathbb{R}^d$ *and the stress field* $\mathbf{\Pi} : \Omega \times (0, T) \to \mathbb{M}^d$ *such that*

$$\mathbf{\Pi}(\mathbf{F}, \dot{\mathbf{F}}) = \mathbf{\Pi}^e(\mathbf{F}) + \mathbf{\Pi}^v(\mathbf{F}, \dot{\mathbf{F}}) \quad \text{in} \quad \Omega \times (0, T), \tag{2.22}$$

$$\rho\ddot{\mathbf{u}} - \operatorname{Div} \mathbf{\Pi} = \mathbf{f} \quad \text{in} \quad \Omega \times (0, T), \tag{2.23}$$

$$\mathbf{u} = \mathbf{0} \quad \text{on} \quad \partial_0\Omega \times (0, T), \tag{2.24}$$

$$\mathbf{\Pi}\boldsymbol{\nu} = \mathbf{g} \quad \text{on} \quad \partial_g\Omega \times (0, T), \tag{2.25}$$

$$\begin{cases} d_{\boldsymbol{\nu}} > 0, & \Gamma_{\boldsymbol{\nu}} = 0; \\ d_{\boldsymbol{\nu}} = 0, & \overset{\circ}{d}_{\boldsymbol{\nu}} \geq 0; \;\; \Gamma_{\boldsymbol{\nu}} \leq 0; \;\; \overset{\circ}{d}_{\boldsymbol{\nu}} \, \Gamma_{\boldsymbol{\nu}} = 0 \end{cases} \quad \text{on} \quad \partial_c\Omega \times (0, T), \tag{2.26}$$

$$\begin{cases} \overset{\circ}{\mathbf{d}}_{\boldsymbol{\tau}} = \|\overset{\circ}{\mathbf{d}}_{\boldsymbol{\tau}}\| \frac{\mathbf{\Gamma}_{\boldsymbol{\tau}}}{\|\mathbf{\Gamma}_{\boldsymbol{\tau}}\|}, \\ \|\mathbf{\Gamma}_{\boldsymbol{\tau}}\| + \mu\Gamma_{\boldsymbol{\nu}} \leq 0, \\ \|\overset{\circ}{\mathbf{d}}_{\boldsymbol{\tau}}\|(\|\mathbf{\Gamma}_{\boldsymbol{\tau}}\| + \mu\Gamma_{\boldsymbol{\nu}}) = 0 \end{cases} \quad \text{on} \quad \partial_c\Omega \times (0, T), \tag{2.27}$$

$$\mathbf{u}(0) = \mathbf{u}_0, \;\; \dot{\mathbf{u}}(0) = \mathbf{u}_1 \quad \text{in} \quad \Omega. \tag{2.28}$$

2.3. Variational Formulation

The variational formulation of problem $\mathcal{P}_S^c$, denoted by $\mathcal{P}_V^c$, is the following.

Problem $\mathcal{P}_V^c$. *Find* $\mathbf{u} \in L^2(0, T; V)$, $\mathbf{\Pi}^e \in L^2(0, T; \mathbb{M}^d)$, $\mathbf{\Pi}^v \in L^2(0, T; \mathbb{M}^d)$, $\Gamma_{\boldsymbol{\nu}} \in L^2(0, T; V^*)$, *and* $\mathbf{\Gamma}_{\boldsymbol{\tau}} \in$

$L^2(0,T;V^*)$*, such that, for all* $t \in (0,T)$*,*

$$\begin{cases} \displaystyle\int_\Omega \rho\ddot{\mathbf{u}} \cdot \mathbf{v}\,\mathrm{d}x + \int_\Omega \mathbf{\Pi} : \nabla\mathbf{v}\,\mathrm{d}x + \mathrm{P}_{c+f}(\mathbf{u},\mathbf{v}) = \int_{\partial_g\Omega} \mathbf{g}\cdot\mathbf{v}\,\mathrm{d}a + \int_\Omega \mathbf{f}\cdot\mathbf{v}\,\mathrm{d}x \quad \forall \mathbf{v} \in V, \\ \mathbf{u}(0) = \mathbf{u}_0, \quad \dot{\mathbf{u}}(0) = \mathbf{u}_1, \end{cases} \tag{2.29}$$

where the space $V = V^{(1)} \times V^{(2)}$ is the space of test fields, with $V^{(i)} = \{\mathbf{v}^{(i)} \in H^1(\Omega^{(i)})^d : \mathbf{v}^{(i)} = \mathbf{0} \text{ on } \partial_0\Omega^{(i)}\}$ and V^* stands for either $H^{-1/2}(\partial_c\Omega)$ or $H^{-1/2}(\partial_c\Omega)^d$, with the addition of the persistence condition combined with the unilateral contact law (2.26), and

$$\mathrm{P}_{c+f}(\mathbf{u},\mathbf{v}) \coloneqq \int_{\partial_c\Omega} (\Gamma_{\boldsymbol{\nu}}\delta d_{\boldsymbol{\nu}} + \mathbf{\Gamma}_{\boldsymbol{\tau}} \cdot \delta\mathbf{d}_{\boldsymbol{\tau}})\,\mathrm{d}a, \tag{2.30}$$

where we have used the following notation:

$$\mathbf{\Pi}\boldsymbol{\nu} = \Gamma_{\boldsymbol{\nu}}\boldsymbol{\nu} + \mathbf{\Gamma}_{\boldsymbol{\tau}} \quad \text{and} \quad \mathbf{\Pi}\boldsymbol{\nu}\cdot\mathbf{v} = \Gamma_{\boldsymbol{\nu}} v_{\boldsymbol{\nu}} + \mathbf{\Gamma}_{\boldsymbol{\tau}}\cdot\mathbf{v}_{\boldsymbol{\tau}},$$

whereas $\delta d_{\boldsymbol{\nu}}$ and $\delta\mathbf{d}_{\boldsymbol{\tau}}$ represent, respectively, the derivatives along direction $\mathbf{v}$ of $d_{\boldsymbol{\nu}}$ and $\mathbf{d}_{\boldsymbol{\tau}}$, regarded as functions of $\mathbf{u}$:

$$\begin{aligned} \delta d_{\boldsymbol{\nu}} &\coloneqq \lim_{\alpha\to 0} \frac{d_{\boldsymbol{\nu}}(\mathbf{u}+\alpha\mathbf{v}) - d_{\boldsymbol{\nu}}(\mathbf{u})}{\alpha} = \boldsymbol{\nu}\cdot\left(\mathbf{v}^{(1)} - \mathbf{v}^{\perp(2)}\right), \\ \delta\mathbf{d}_{\boldsymbol{\tau}} &\coloneqq \lim_{\alpha\to 0} \frac{\mathbf{d}_{\boldsymbol{\tau}}(\mathbf{u}+\alpha\mathbf{v}) - \mathbf{d}_{\boldsymbol{\tau}}(\mathbf{u})}{\alpha} = (\mathbf{I} - \boldsymbol{\nu}\otimes\boldsymbol{\nu})\left(\mathbf{v}^{(1)} - \mathbf{v}^{\perp(2)}\right), \end{aligned} \tag{2.31}$$

$$\text{where } \mathbf{v}^{(1)} = \mathbf{v}^{(1)}\left(\mathbf{x}^{(1)}\right) \text{ and } \mathbf{v}^{\perp(2)} = \mathbf{v}^{(2)}\left(\mathbf{x}^{\perp(2)}\right). \tag{2.32}$$

2.4. Conservation and dissipation properties in the continuous case

From a physical point of view, the solution of a hyper-elastodynamic problem has to satisfy suitable conservation properties such as energy balance, linear momentum balance, and angular momentum balance. In the absence of contact and friction, energy conservation can be written as

$$\int_0^t \dot{E}(s)\mathrm{d}s = E(t) - E(0) = \int_0^t \int_\Omega \mathbf{f}\cdot\dot{\mathbf{u}}\,\mathrm{d}x\,\mathrm{d}s \;+\; \int_0^t \int_{\partial_g\Omega} \mathbf{g}\cdot\dot{\mathbf{u}}\,\mathrm{d}a\,\mathrm{d}s, \tag{2.33}$$

where $(s,t) \in (0,T)\times(0,T)$ and $E(t)$ denotes the total mechanical energy of the two-body system, defined as:

$$E(t) = \frac{1}{2}\int_\Omega \rho\|\dot{\mathbf{u}}\|^2\,\mathrm{d}x + \int_\Omega \widetilde{W}(\mathbf{C})\,\mathrm{d}x \tag{2.34}$$

with $\widetilde{W}$ the volume elastic energy for the two-body system, and $\mathbf{C} = \mathbf{F}^T\mathbf{F}$ is the right Cauchy–Green tensor.
When the problem is extended to viscosity, as well as to contact phenomena with friction, energy balance takes the form:

$$\begin{aligned} \int_0^t \dot{E}(s)\mathrm{d}s = E(t) - E(0) = \int_0^t \int_\Omega \mathbf{f}\cdot\dot{\mathbf{u}}\,\mathrm{d}x\,\mathrm{d}s \;+\; \int_0^t \int_{\partial_g\Omega} \mathbf{g}\cdot\dot{\mathbf{u}}\,\mathrm{d}a\,\mathrm{d}s \\ - \int_0^t \mathrm{P}_{c+f}(\mathbf{u},\dot{\mathbf{u}})\,\mathrm{d}s - \int_0^t \int_\Omega \mathbf{\Pi}^v : \nabla\dot{\mathbf{u}}\,\mathrm{d}x\mathrm{d}s \end{aligned} \tag{2.35}$$

Equation (2.35) results in fact from the time integration of the weak formulation (2.29) between 0 and t with the virtual field $\mathbf{v}$ equal to the actual velocity field $\dot{\mathbf{u}}$, i.e.:

$$\int_0^t \int_\Omega \rho \ddot{\mathbf{u}} \cdot \dot{\mathbf{u}} \, \mathrm{d}x\mathrm{d}s + \int_0^t \int_\Omega \mathbf{\Pi}^e : \nabla \dot{\mathbf{u}} \, \mathrm{d}x\mathrm{d}s + \int_0^t \int_\Omega \mathbf{\Pi}^v : \nabla \dot{\mathbf{u}} \, \mathrm{d}x\mathrm{d}s$$
$$= \int_0^t \int_{\partial_g \Omega} \mathbf{g} \cdot \dot{\mathbf{u}} \ \mathrm{d}a\mathrm{d}s + \int_0^t \int_\Omega \mathbf{f} \cdot \dot{\mathbf{u}} \, \mathrm{d}x\mathrm{d}s - \int_0^t \mathrm{P}_{c+f}(\mathbf{u}, \dot{\mathbf{u}}) \mathrm{d}s \quad (2.36)$$

where the frictional contact stress actual power $\mathcal{W}_{c+f}(t)$ is

$$\mathcal{W}_{c+f}(t) \coloneqq \mathrm{P}_{c+f}(\mathbf{u}, \dot{\mathbf{u}}) = \int_{\partial_c \Omega} (\Gamma_{\boldsymbol{\nu}} \overset{\circ}{d}_{\boldsymbol{\nu}} + \mathbf{\Gamma}_{\boldsymbol{\tau}} \cdot \overset{\circ}{\mathbf{d}}_{\boldsymbol{\tau}}) \, \mathrm{d}a, \quad (2.37)$$

$\overset{\circ}{d}_{\boldsymbol{\nu}}$ and $\overset{\circ}{\mathbf{d}}_{\boldsymbol{\tau}}$ respectively representing the material time derivatives of $d_{\boldsymbol{\nu}}$ and $\mathbf{d}_{\boldsymbol{\tau}}$ (see (2.7) and (2.8)). The *dissipation* associated with viscosity is

$$D(t) \coloneqq \int_\Omega \mathbf{\Pi}^v : \nabla \dot{\mathbf{u}} \, \mathrm{d}x.$$

In the case of persistent contact and depending on the presence of friction and viscosity, the energy balance given by (2.35) can be either conservative or dissipative. In the absence of external forces, (2.35) becomes:

$$E(t) - E(0) = -\int_0^t \mathcal{W}_{c+f}(s) \, \mathrm{d}s - \int_0^t D(s) \, \mathrm{d}s$$

Taking into account the Legendre–Hadamard condition $\mathbf{\Pi}^v(\mathbf{F}, \dot{\mathbf{F}}) : \dot{\mathbf{F}} \geq \mathbf{0}$, we can distinguish four cases:

1. Case without friction and without viscosity:

$$\Gamma_{\boldsymbol{\nu}} \overset{\circ}{d}_{\boldsymbol{\nu}} = 0 \text{ and } \mathbf{\Gamma}_{\boldsymbol{\tau}} \cdot \overset{\circ}{\mathbf{d}}_{\boldsymbol{\tau}} = 0 \Rightarrow \mathcal{W}_{c+f} = 0 \Rightarrow E(0) = E(t) \ \text{ with } D = 0. \quad (2.38)$$

2. Case without friction and with viscosity:

$$\Gamma_{\boldsymbol{\nu}} \overset{\circ}{d}_{\boldsymbol{\nu}} = 0 \text{ and } \mathbf{\Gamma}_{\boldsymbol{\tau}} \cdot \overset{\circ}{\mathbf{d}}_{\boldsymbol{\tau}} = 0 \Rightarrow \mathcal{W}_{c+f} = 0 \Rightarrow \ E(t) - E(0) = -\int_0^t \int_\Omega \underbrace{\mathbf{\Pi}^v : \nabla \dot{\mathbf{u}}}_{\geq 0} \, \mathrm{d}x\mathrm{d}s \leq 0 \quad \Rightarrow E(0) \geq E(t). \quad (2.39)$$

3. Case with friction and without viscosity:

$$\Gamma_{\boldsymbol{\nu}} \overset{\circ}{d}_{\boldsymbol{\nu}} = 0 \text{ and } \mathbf{\Gamma}_{\boldsymbol{\tau}} \cdot \overset{\circ}{\mathbf{d}}_{\boldsymbol{\tau}} \geq 0 \Rightarrow \mathcal{W}_{c+f} \geq 0 \Rightarrow \ E(0) \geq E(t) \ \text{ with } D = 0. \quad (2.40)$$

4. Case with friction and with viscosity:

$$\Gamma_{\boldsymbol{\nu}} \overset{\circ}{d}_{\boldsymbol{\nu}} = 0 \text{ and } \mathbf{\Gamma}_{\boldsymbol{\tau}} \cdot \overset{\circ}{\mathbf{d}}_{\boldsymbol{\tau}} \geq 0 \Rightarrow \mathcal{W}_{c+f} \geq 0$$
$$\Rightarrow E(t) - E(0) = -\int_0^t \underbrace{\mathcal{W}_{c+f}(s)}_{\geq 0} \mathrm{d}s - \int_0^t \int_\Omega \underbrace{\mathbf{\Pi}^v : \nabla \dot{\mathbf{u}}}_{\geq 0} \, \mathrm{d}x\mathrm{d}s \leq 0 \Rightarrow E(0) \geq E(t). \quad (2.41)$$

The case (2.38) means that the persistence condition (2.9) implies the total conservation of energy. On the other hand when the contact is with friction or with viscosity (2.39)–(2.40)–(2.41), the dissipation of energy occurring between $t = 0$ and the current time t corresponds to the dissipative phenomenon of friction and viscosity.

3. Energy-consistent numerical approach

In this section, we devise a numerical approximation in adequacy with the energy consistency of the hyperelastic frictional contact system with an extension to viscosity, and in agreement with the continuous framework. Indeed, several numerical approximations can give rise to a dissipation or an increase in energy, which are not physically acceptable at the continuous level [14, 7].

3.1. The usual discrete energy conservation framework

First of all, we recall in this section the usual discrete energy conservation framework in the no-contact case. When non-linear dynamics problems are considered, the standard implicit schemes (θ-method, Newmark schemes, midpoint or HHT methods, see for example [68, 7, 8, 13]) lose their unconditional stability. We therefore need to use implicit energy conservation approaches [7, 8, 14, 13, 37, 57] which are appropriate due to their accuracy and long-time integration stability. These methods are devised in such a way that discrete energy conservation properties are satisfied. In what follows, we consider a discrete set of times $(t_i)_{i=0,\dots,N}$ which defines a partition of the time interval $[0,T] = \cup_{i=0}^{N-1}[t_i, t_{i+1}]$ with $t_{i+1} = t_i + \Delta t$ and $\Delta t = \dfrac{T}{N}$. Using the second-order time integration system (midpoint scheme) with energy conservation properties [14], the weak form of a non-linear hyper-visco-elastodynamic problem integrated between times t_i and t_{i+1} gives the following system:

$$\begin{cases} \text{Find } \mathbf{u}_{i+1} \in U \text{ such that} \\ \dfrac{1}{\Delta t}\displaystyle\int_\Omega \rho(\dot{\mathbf{u}}_{i+1} - \dot{\mathbf{u}}_i)\cdot\mathbf{v}\ \mathrm{d}x + \int_\Omega \mathbf{\Pi}^e_{\text{algo}} : \nabla\mathbf{v}\ \mathrm{d}x + \int_\Omega \mathbf{\Pi}^v_{i+\frac{1}{2}} : \nabla\mathbf{v}\ \mathrm{d}x - \int_\Omega \mathbf{f}_{i+\frac{1}{2}}\cdot\mathbf{v}\ \mathrm{d}x - \int_{\partial_g\Omega} \mathbf{g}_{i+\frac{1}{2}}\cdot\mathbf{v}\,\mathrm{d}a = 0. \end{cases} \tag{3.1}$$

with $\dot{\mathbf{u}}_{i+1} \coloneqq \dot{\mathbf{u}}_i + \Delta t\,\ddot{\mathbf{u}}_{i+1/2}$. In (3.1), $\square_{i+\frac{1}{2}} = \frac{1}{2}(\square_i + \square_{i+1})$ and $\square_i$ denotes an approximation of $\square(t_i)$. Moreover, the time integration scheme (3.1) used in this work is characterized by the tensor $\mathbf{\Pi}^e_{\text{algo}}$ proposed by Gonzalez [14] and defined by:

$$\begin{cases} \mathbf{\Pi}^e_{\text{algo}} = \mathbf{F}_{i+\frac{1}{2}}\sum_{\text{algo}}, \\ \sum_{\text{algo}} = 2\dfrac{\partial\tilde{W}}{\partial\mathbf{C}}(\mathbf{C}_{i+\frac{1}{2}}) + 2[\widetilde{W}(\mathbf{C}_{i+1}) - \widetilde{W}(\mathbf{C}_i) - \dfrac{\partial\tilde{W}}{\partial\mathbf{C}}(\mathbf{C}_{i+\frac{1}{2}}) : \Delta\mathbf{C}_i]\dfrac{\Delta\mathbf{C}_i}{\Delta\mathbf{C}_i : \Delta\mathbf{C}_i}, \end{cases} \tag{3.2}$$

with $\Delta\mathbf{C}_i = \mathbf{C}_{i+1} - \mathbf{C}_i$ and $\mathbf{C}_i = \mathbf{F}_i^T\mathbf{F}_i$. The previous relations (3.2) were introduced in order to satisfy energy conservation under the following form (see [14]):

$$\mathbf{\Pi}^e_{\text{algo}} : (\nabla\mathbf{u}_{i+1} - \nabla\mathbf{u}_i) = \widetilde{W}(\mathbf{C}_{i+1}) - \widetilde{W}(\mathbf{C}_i). \tag{3.3}$$

Furthemore, several relevant references concerning energy-momentum conserving schemes for general hyperelastic models have demonstrated their validity [18, 19, 20, 21].

3.2. Approach adapted to frictional contact

Many works have been devoted to extend these conservative formulations to frictionless impact; more precisely, Laursen & Chawla [25] and Amero & Petocz [26] have shown the benefit of the persistence condition to conserve the energy in the discrete framework. But these works are characterized by a contact interpenetration that can only vanish when the time step tends to zero. In order to overcome this drawback Laursen & Love [15] have developed an efficient method by introducing a discrete jump in velocity; but this method requires the solution of an auxilary system in order to compute the velocity update results. Further developments, also within the contact framework,

can be found in Hauret & Le Tallec [16], Haikal & Hjelmstad [36], Betsch & Hesch [29], and Hesch & Betsch [30]. Applications of the energy-momentum scheme using the mortar method can be found in Hesch & Betsch [69] for transient 3D domain decomposition problems, in Hesch & Betsch [32] for two-dimensional contact problems, and in Hesch & Betsch [31] and Puso & Laursen [35] for three-dimensional contact problems.
In this section, we present an energy-consistent algorithm for hyper-visco-elastodynamic contact problems that differs from the approaches mentioned above. Indeed, this method makes it possible to apply the Kuhn–Tucker conditions in displacement and the persistence condition during each time step at low computational cost, and allowing for a slight contact penetration. We term this method *midpoint scheme with leapfrog procedure*.
In order to take into account contact at time $t_{i+\frac{1}{2}}$, we choose to implicitly approximate the contact term with friction (2.30); thus the weak form (2.29) integrated between times t_i and t_{i+1} can be written as:

$$\begin{cases} \text{Find } \mathbf{u}_{i+1} \in U \text{ such that} \\ \dfrac{1}{\Delta t}\displaystyle\int_\Omega \rho(\dot{\mathbf{u}}_{i+1} - \dot{\mathbf{u}}_p)\cdot\mathbf{v}\ \mathrm{d}x + \int_\Omega \mathbf{\Pi}^e_{\text{algo}} : \nabla\mathbf{v}\ \mathrm{d}x + \int_\Omega \mathbf{\Pi}^v_{i+\frac{1}{2}} : \nabla\mathbf{v}\ \mathrm{d}x - \int_\Omega \mathbf{f}_{i+\frac{1}{2}}\cdot\mathbf{v}\ \mathrm{d}x - \int_{\partial_g\Omega}\mathbf{g}_{i+\frac{1}{2}}\cdot\mathbf{v}\ \mathrm{d}a \\ \qquad + \displaystyle\int_{\partial_c\Omega}(\Gamma_{\boldsymbol{\nu}_{i+\frac{1}{2}}}\delta d_{\boldsymbol{\nu}_{i+\frac{1}{2}}} + \mathbf{\Gamma}_{\boldsymbol{\tau}_{i+\frac{1}{2}}}\cdot\delta\mathbf{d}_{\boldsymbol{\tau}_{i+\frac{1}{2}}})\ \mathrm{d}a = 0, \end{cases} \tag{3.4}$$

where $\delta d_{\boldsymbol{\nu}_{i+\frac{1}{2}}} = \boldsymbol{\nu}_{i+\frac{1}{2}}\cdot(\mathbf{v}^{(1)} - \mathbf{v}^{\perp(2)})$, and $\delta\mathbf{d}_{\boldsymbol{\tau}_{i+\frac{1}{2}}} = (\mathbf{I} - \boldsymbol{\nu}_{i+\frac{1}{2}}\otimes\boldsymbol{\nu}_{i+\frac{1}{2}})(\mathbf{v}^{(1)} - \mathbf{v}^{\perp(2)})$.
Thus, the approximation of the frictional contact term provided in (3.4) leads us to applying the frictional contact conditions at time $t_{i+\frac{1}{2}}$, that is, the discrete versions of the unilateral contact law, of Coulomb's friction law, and of the persistent contact law. The discrete form of the normal and tangential contact distances are defined respectively by:

$$\begin{cases} d_{\boldsymbol{\nu}_{i+\frac{1}{2}}} \coloneqq \boldsymbol{\nu}_{i+\frac{1}{2}}\cdot(\mathbf{x}^{(1)} + \mathbf{u}^{(1)}_{i+\frac{1}{2}}(\mathbf{x}^{(1)},t) - (\mathbf{x}^{\perp(2)} + \mathbf{u}^{(2)}_{i+\frac{1}{2}}(\mathbf{x}^{\perp(2)},t))), \\ \mathbf{d}_{\boldsymbol{\tau}_{i+\frac{1}{2}}} \coloneqq (\mathbf{I} - \boldsymbol{\nu}_{i+\frac{1}{2}}\otimes\boldsymbol{\nu}_{i+\frac{1}{2}})(\mathbf{x}^{(1)} + \mathbf{u}^{(1)}_{i+\frac{1}{2}}(\mathbf{x}^{(1)},t) - (\mathbf{x}^{\perp(2)} + \mathbf{u}^{(2)}_{i+\frac{1}{2}}(\mathbf{x}^{\perp(2)},t))). \end{cases} \tag{3.5}$$

We also consider the following discrete forms of the normal and tangential contact velocities ($\overset{\circ}{d}_{\boldsymbol{\nu}}$, $\overset{\circ}{\mathbf{d}}_{\boldsymbol{\tau}}$) at time $t_{i+\frac{1}{2}}$:

$$\begin{cases} \delta_{i+\frac{1}{2}}\overset{\circ}{d}_{\boldsymbol{\nu}_{i+\frac{1}{2}}} \coloneqq \dfrac{d_{\boldsymbol{\nu}_{i+1}} - d_{\boldsymbol{\nu}_i}}{\Delta t}, \\ \delta_{i+\frac{1}{2}}\overset{\circ}{\mathbf{d}}_{\boldsymbol{\tau}_{i+\frac{1}{2}}} \coloneqq \dfrac{\mathbf{d}_{\boldsymbol{\tau}_{i+1}} - \mathbf{d}_{\boldsymbol{\tau}_i}}{\Delta t}, \end{cases} \tag{3.6}$$

where the notation $\delta_{i+\frac{1}{2}}\square$ represents the incremental discretization of $\square$ at time $t_{i+\frac{1}{2}}$.

3.2.1. Midpoint time-integration scheme with leapfrog procedure

The strategy developed to solve the system (3.4) is based on the application of the persistent contact law during each time step; this is possible by applying the unilateral displacement condition and the persistent contact condition during the transition from t_i to t_{i+1}. To do this, we developed a midpoint scheme for the persistent contact condition at time $t_{i+\frac{1}{2}}$ combined with the leapfrog procedure for the normal contact distance. Moreover, we have Coulomb's friction law at discrete time $t_{i+\frac{1}{2}}$.We propose the following midpoint time-integration scheme with leapfrog procedure:

$$\begin{cases} \text{if } d^{\text{Leapfrog}}_{\boldsymbol{\nu}_{i+\frac{1}{2}}} > 0 \quad \Gamma_{\boldsymbol{\nu}_{i+\frac{1}{2}}} = 0; \\ \text{if } d^{\text{Leapfrog}}_{\boldsymbol{\nu}_{i+\frac{1}{2}}} = 0 \quad \delta_{i+\frac{1}{2}}\overset{\circ}{d}_{\boldsymbol{\nu}_{i+\frac{1}{2}}} \geq 0;\ \Gamma_{\boldsymbol{\nu}_{i+\frac{1}{2}}} \leq 0;\ \delta_{i+\frac{1}{2}}\overset{\circ}{d}_{\boldsymbol{\nu}_{i+\frac{1}{2}}}\ \Gamma_{\boldsymbol{\nu}_{i+\frac{1}{2}}} = 0 \\ \qquad\qquad \delta_{i+\frac{1}{2}}\overset{\circ}{\mathbf{d}}_{\boldsymbol{\tau}_{i+\frac{1}{2}}} = \|\delta_{i+\frac{1}{2}}\overset{\circ}{\mathbf{d}}_{\boldsymbol{\tau}_{i+\frac{1}{2}}}\|\frac{\mathbf{\Gamma}_{\boldsymbol{\tau}_{i+\frac{1}{2}}}}{\|\mathbf{\Gamma}_{\boldsymbol{\tau}_{i+\frac{1}{2}}}\|};\ \|\mathbf{\Gamma}_{\boldsymbol{\tau}_{i+\frac{1}{2}}}\| + \mu\Gamma_{\boldsymbol{\nu}_{i+\frac{1}{2}}} \leq 0; \\ \qquad\qquad \|\delta_{i+\frac{1}{2}}\overset{\circ}{\mathbf{d}}_{\boldsymbol{\tau}_{i+\frac{1}{2}}}\|\,(\|\mathbf{\Gamma}_{\boldsymbol{\tau}_{i+\frac{1}{2}}}\| + \mu\Gamma_{\boldsymbol{\nu}_{i+\frac{1}{2}}}) = 0, \end{cases} \tag{3.7}$$

with $d_{\boldsymbol{\nu}_{i+\frac{1}{2}}^{\text{Leapfrog}}} \coloneqq d_{\boldsymbol{\nu}_i} + \frac{\Delta t}{2}\delta_i d_{\boldsymbol{\nu}_i}$, and $\delta_i d_{\boldsymbol{\nu}_i} \coloneqq (d_{\boldsymbol{\nu}_i} - d_{\boldsymbol{\nu}_{i-1}})/\Delta t$.

3.2.2. Evolution of the discrete energy

The objective of this section is to perform the analysis of the evolution of the discrete energy in relation to the numerical approach presented in the previous section. To do this, we have established the following result which represents the evaluation of the discrete energy between the instants t_i and t_{i+1}.

Proposition 3.1. *It holds*

$$E_{i+1} - E_i = \Delta t \int_\Omega \mathbf{f}_{i+\frac{1}{2}} \cdot \dot{\mathbf{u}}_{i+\frac{1}{2}} \, \mathrm{d}x + \Delta t \int_{\partial_g \Omega} \mathbf{g}_{i+\frac{1}{2}} \cdot \dot{\mathbf{u}}_{i+\frac{1}{2}} \, \mathrm{d}a - \Delta t \int_{\partial_c \Omega} (\Gamma_{\boldsymbol{\nu}_{i+\frac{1}{2}}} \delta \overset{\circ}{d}_{\boldsymbol{\nu}_{i+\frac{1}{2}}} + \boldsymbol{\Gamma}_{\boldsymbol{\tau}_{i+\frac{1}{2}}} \cdot \delta \overset{\circ}{\mathbf{d}}_{\boldsymbol{\tau}_{i+\frac{1}{2}}}) \, \mathrm{d}a - D_{i+\frac{1}{2}} \tag{3.8}$$

with

$$D_{i+\frac{1}{2}} \coloneqq \Delta t \int_\Omega \boldsymbol{\Pi}^v : \nabla \dot{\mathbf{u}}_{i+\frac{1}{2}} \, \mathrm{d}x, \tag{3.9}$$

where E_i and E_{i+1} denote respectively the mechanical energy E at times t_i and t_{i+1}. For example, the discrete energy E_{i+1} can be written as:

$$E_{i+1} = \frac{1}{2} \int_\Omega \rho \|\dot{\mathbf{u}}_{i+1}\|^2 \, \mathrm{d}x + \int_\Omega \widetilde{W}(\mathbf{C}_{i+1}) \, \mathrm{d}x. \tag{3.10}$$

Proof. Using the variational formulation (3.4) with $\mathbf{v} = \dot{\mathbf{u}}_{i+\frac{1}{2}}$, we have:

$$\frac{1}{\Delta t} \int_\Omega \rho(\dot{\mathbf{u}}_{i+1} - \dot{\mathbf{u}}_i) \cdot \dot{\mathbf{u}}_{i+\frac{1}{2}} \, \mathrm{d}x + \int_\Omega \boldsymbol{\Pi}^e_{\text{algo}} : \nabla \dot{\mathbf{u}}_{i+\frac{1}{2}} \, \mathrm{d}x = \int_\Omega \mathbf{f}_{i+\frac{1}{2}} \cdot \dot{\mathbf{u}}_{i+\frac{1}{2}} \, \mathrm{d}x + \int_{\partial_g \Omega} \mathbf{g}_{i+\frac{1}{2}} \cdot \dot{\mathbf{u}}_{i+\frac{1}{2}} \, \mathrm{d}a$$
$$- \int_{\partial_c \Omega} (\Gamma_{\boldsymbol{\nu}_{i+\frac{1}{2}}} \delta \overset{\circ}{d}_{\boldsymbol{\nu}_{i+\frac{1}{2}}} + \boldsymbol{\Gamma}_{\boldsymbol{\tau}_{i+\frac{1}{2}}} \cdot \delta \overset{\circ}{\mathbf{d}}_{\boldsymbol{\tau}_{i+\frac{1}{2}}}) \, \mathrm{d}a - \int_\Omega \boldsymbol{\Pi}^v_{i+\frac{1}{2}} : \nabla \dot{\mathbf{u}}_{i+\frac{1}{2}} \, \mathrm{d}x$$

where $\overset{\circ}{d}_{\boldsymbol{\nu}_{i+\frac{1}{2}}}$ and $\overset{\circ}{\mathbf{d}}_{\boldsymbol{\tau}_{i+\frac{1}{2}}}$ are given in (3.6).
Using the relation

$$\dot{\mathbf{u}}_{i+\frac{1}{2}} = \frac{\dot{\mathbf{u}}_{i+1} + \dot{\mathbf{u}}_i}{2} = \frac{\mathbf{u}_{i+1} - \mathbf{u}_i}{\Delta t},$$

we obtain

$$\frac{1}{2\Delta t} \int_\Omega \rho(\dot{\mathbf{u}}_{i+1} - \dot{\mathbf{u}}_i) \cdot (\dot{\mathbf{u}}_{i+1} + \dot{\mathbf{u}}_i) \, \mathrm{d}x + \frac{1}{\Delta t} \int_\Omega \boldsymbol{\Pi}^e_{\text{algo}} : \nabla(\mathbf{u}_{i+1} - \mathbf{u}_i) \, \mathrm{d}x = \int_\Omega \mathbf{f}_{i+\frac{1}{2}} \cdot \dot{\mathbf{u}}_{i+\frac{1}{2}} \, \mathrm{d}x + \int_{\partial_g \Omega} \mathbf{g}_{i+\frac{1}{2}} \cdot \dot{\mathbf{u}}_{i+\frac{1}{2}} \, \mathrm{d}a$$
$$- \int_{\partial_c \Omega} (\Gamma_{\boldsymbol{\nu}_{i+\frac{1}{2}}} \delta \overset{\circ}{d}_{\boldsymbol{\nu}_{i+\frac{1}{2}}} + \boldsymbol{\Gamma}_{\boldsymbol{\tau}_{i+\frac{1}{2}}} \cdot \delta \overset{\circ}{\mathbf{d}}_{\boldsymbol{\tau}_{i+\frac{1}{2}}}) \, \mathrm{d}a - \int_\Omega \boldsymbol{\Pi}^v_{i+\frac{1}{2}} : \nabla \dot{\mathbf{u}}_{i+\frac{1}{2}} \, \mathrm{d}x.$$

Also, using the identity $(\dot{\mathbf{u}}_{i+1} - \dot{\mathbf{u}}_i) \cdot (\dot{\mathbf{u}}_{i+1} + \dot{\mathbf{u}}_i) = \|\dot{\mathbf{u}}_{i+1}\|^2 - \|\dot{\mathbf{u}}_i\|^2$ and the conservation property of Gonzalez's scheme given by (3.3), we get:

$$\frac{1}{2\Delta t} \int_\Omega \rho(\|\dot{\mathbf{u}}_{i+1}\|^2 - \|\dot{\mathbf{u}}_i\|^2) \, \mathrm{d}x + \frac{1}{\Delta t} \int_\Omega \widetilde{W}(\mathbf{C}_{i+1}) - \widetilde{W}(\mathbf{C}_i) \, \mathrm{d}x = \int_\Omega \mathbf{f}_{i+\frac{1}{2}} \cdot \dot{\mathbf{u}}_{i+\frac{1}{2}} \, \mathrm{d}x + \int_{\partial_g \Omega} \mathbf{g}_{i+\frac{1}{2}} \cdot \dot{\mathbf{u}}_{i+\frac{1}{2}} \, \mathrm{d}a$$
$$- \int_{\partial_c \Omega} (\Gamma_{\boldsymbol{\nu}_{i+\frac{1}{2}}} \delta \overset{\circ}{d}_{\boldsymbol{\nu}_{i+\frac{1}{2}}} + \boldsymbol{\Gamma}_{\boldsymbol{\tau}_{i+\frac{1}{2}}} \cdot \delta \overset{\circ}{\mathbf{d}}_{\boldsymbol{\tau}_{i+\frac{1}{2}}}) \, \mathrm{d}a - \int_\Omega \boldsymbol{\Pi}^v : \nabla \dot{\mathbf{u}}_{i+\frac{1}{2}} \, \mathrm{d}x.$$

Finally, using the definition (3.10) of discrete energy, we have:

$$E_{i+1} - E_i = \frac{1}{2}\int_\Omega \rho(\|\dot{\mathbf{u}}_{i+1}\|^2 - \|\dot{\mathbf{u}}_i\|^2)\ \mathrm{d}x + \int_\Omega \widetilde{W}(\mathbf{C}_{i+1}) - \widetilde{W}(\mathbf{C}_i)\ \mathrm{d}x$$
$$= \Delta t \int_\Omega \mathbf{f}_{i+\frac{1}{2}} \cdot \dot{\mathbf{u}}_{i+\frac{1}{2}}\ \mathrm{d}x + \Delta t \int_{\partial_g\Omega} \mathbf{g}_{i+\frac{1}{2}} \cdot \dot{\mathbf{u}}_{i+\frac{1}{2}}\ \mathrm{d}a - \Delta t \int_{\partial_c\Omega} (\Gamma_{\boldsymbol{\nu}_{i+\frac{1}{2}}} \overset{\circ}{\delta d}_{\boldsymbol{\nu}_{i+\frac{1}{2}}} + \boldsymbol{\Gamma}_{\boldsymbol{\tau}_{i+\frac{1}{2}}} \cdot \overset{\circ}{\delta \mathbf{d}}_{\boldsymbol{\tau}_{i+\frac{1}{2}}})\ \mathrm{d}a - D_{i+\frac{1}{2}}.$$

□

When the external forces are assumed to be zero, we obtain:

$$E_{i+1} - E_i = -\Delta t \int_{\partial_c\Omega} (\Gamma_{\boldsymbol{\nu}_{i+\frac{1}{2}}} \overset{\circ}{\delta d}_{\boldsymbol{\nu}_{i+\frac{1}{2}}} + \boldsymbol{\Gamma}_{\boldsymbol{\tau}_{i+\frac{1}{2}}} \cdot \overset{\circ}{\delta \mathbf{d}}_{\boldsymbol{\tau}_{i+\frac{1}{2}}})\ \mathrm{d}a - D_{i+\frac{1}{2}}. \tag{3.11}$$

Taking into account the midpoint scheme with leapfrog procedure and the fact that $D \geq 0$ for any time, so that $D_{i+\frac{1}{2}} \approx D(t_{i+\frac{1}{2}}) \geq 0$, the energy balance reads as follows.

1. Case without friction and without viscosity:

$$\Gamma_{\boldsymbol{\nu}_{i+\frac{1}{2}}} \overset{\circ}{\delta d}_{\boldsymbol{\nu}_{i+\frac{1}{2}}} = 0 \text{ and } \boldsymbol{\Gamma}_{\boldsymbol{\tau}_{i+\frac{1}{2}}} \cdot \overset{\circ}{\delta \mathbf{d}}_{\boldsymbol{\tau}_{i+\frac{1}{2}}} = 0 \text{ with } D_{i+\frac{1}{2}} = 0 \Rightarrow E_i = E_{i+1}. \tag{3.12}$$

2. Case without friction and with viscosity:

$$\Gamma_{\boldsymbol{\nu}_{i+\frac{1}{2}}} \overset{\circ}{\delta d}_{\boldsymbol{\nu}_{i+\frac{1}{2}}} = 0 \text{ and } \boldsymbol{\Gamma}_{\boldsymbol{\tau}_{i+\frac{1}{2}}} \cdot \overset{\circ}{\delta \mathbf{d}}_{\boldsymbol{\tau}_{i+\frac{1}{2}}} = 0 \text{ with } D_{i+\frac{1}{2}} \geq 0 \Rightarrow E_i \geq E_{i+1}. \tag{3.13}$$

3. Case with friction and without viscosity:

$$\Gamma_{\boldsymbol{\nu}_{i+\frac{1}{2}}} \overset{\circ}{\delta d}_{\boldsymbol{\nu}_{i+\frac{1}{2}}} = 0 \text{ and } \boldsymbol{\Gamma}_{\boldsymbol{\tau}_{i+\frac{1}{2}}} \cdot \overset{\circ}{\delta \mathbf{d}}_{\boldsymbol{\tau}_{p+\frac{1}{2}}} \geq 0 \text{ with } D_{i+\frac{1}{2}} = 0 \Rightarrow E_i \geq E_{i+1}. \tag{3.14}$$

4. Case with friction and with viscosity:

$$\Gamma_{\boldsymbol{\nu}_{i+\frac{1}{2}}} \overset{\circ}{\delta d}_{\boldsymbol{\nu}_{i+\frac{1}{2}}} = 0 \text{ and } \boldsymbol{\Gamma}_{\boldsymbol{\tau}_{i+\frac{1}{2}}} \cdot \overset{\circ}{\delta \mathbf{d}}_{\boldsymbol{\tau}_{i+\frac{1}{2}}} \geq 0 \text{ with } D_{i+\frac{1}{2}} \geq 0 \Rightarrow E_i \geq E_{i+1}. \tag{3.15}$$

As a result, this strategy allows for an exact energy conservation between times t_i and t_{i+1} when friction and viscosity are not considered and moreover, it allows for a dissipation of the energy in adequacy with the continuous case when friction and viscosity are taken into account.

4. Variational approximation

This section is devoted to the discretization of the variational problem $\mathcal{P}_V^c$. Let Ω be a polyhedral domain. Consider a regular partition $\mathcal{T}^h$ of triangular finite elements of $\overline{\Omega}$ which are compatible with the boundary decomposition $\partial\Omega = \overline{\partial_0\Omega} \cup \overline{\partial_g\Omega} \cup \overline{\partial_c\Omega}$, i.e., if one side of an element $K \in \mathcal{T}^h$ has more than a point on $\partial\Omega$, then the side lies entirely on $\overline{\partial_0\Omega}$, $\overline{\partial_g\Omega}$ or $\overline{\partial_c\Omega}$. The space V is approximated by the finite dimensional space $V^h \subset V$ of continuous and piecewise polynomial functions:

$$V^h := \{\mathbf{v}^h \in [C(\overline{\Omega})]^d\ :\ \mathbf{v}^h|_K \in \mathbb{P}_k(K)^d\ \ \forall\, K \in \mathcal{T}^h,\ \mathbf{v}^h = \mathbf{0} \text{ on } \partial_c\Omega\},$$

where $\mathbb{P}_k(K)$ represents the space of polynomials of degree less than or equal to $k \in \mathbb{N}$ in K and $h > 0$ is the mesh size. The elements $\mathbf{u}_0^h \in V^h$ and $\mathbf{u}_1^h \in V^h$ are the finite element approximations of $\mathbf{u}_0$ and $\mathbf{u}_1$, respectively. Then, using the previous notations and the midpoint scheme, the discrete approximation of the problem $\mathcal{P}_V^c$ at time $t_{i+\frac{1}{2}}$ reads as follows.

Problem $\mathcal{P}_V^{h\Delta t}$. *Find a discrete displacement field* $\mathbf{u}^{h\Delta t} = \{\mathbf{u}_i^{h\Delta t}\}_{i=0}^n \subset V^h$*, a discrete normal stress field* $\Gamma_{\boldsymbol{\nu}}^{h\Delta t} = \{\Gamma_{\boldsymbol{\nu}} i^{h\Delta t}\}_{i=0}^n \subset (V^h)^*$ *and a discrete tangential stress field* $\boldsymbol{\Gamma}_{\boldsymbol{\tau}}^{h\Delta t} = \{\boldsymbol{\Gamma}_{\boldsymbol{\tau}} i^{h\Delta t}\}_{i=0}^n \subset (V^h)^*$ *such that, for all* $i = 0, \dots, n$*,*

$$\frac{1}{\Delta t}\int_\Omega \rho(\dot{\mathbf{u}}_{i+1}^{h\Delta t} - \dot{\mathbf{u}}_i^{h\Delta t}) \cdot \mathbf{v}^h \ \mathrm{d}x + \int_\Omega \boldsymbol{\Pi}_{i+\frac{1}{2}} : \nabla \mathbf{v}^h - \int_\Omega \mathbf{f}_{i+\frac{1}{2}}^{h\Delta t} \cdot \mathbf{v}^h \ \mathrm{d}x - \int_{\partial_g\Omega} \mathbf{g}_{i+\frac{1}{2}}^{h\Delta t} \cdot \mathbf{v}^h \ \mathrm{d}a + \int_{\partial_c\Omega} (\Gamma_{\boldsymbol{\nu}_{i+\frac{1}{2}}}^{h\Delta t} \delta d_{\boldsymbol{\nu}_{p+\frac{1}{2}}}^{h\Delta t} + \boldsymbol{\Gamma}_{\boldsymbol{\tau}_{i+\frac{1}{2}}}^{h\Delta t} \cdot \delta \mathbf{d}_{\boldsymbol{\tau}_{i+\frac{1}{2}}}^{h\Delta t}) \ \mathrm{d}a = 0, \tag{4.1}$$

with frictional contact conditions (3.7),

where $\boldsymbol{\Pi}_{i+\frac{1}{2}} : \nabla \mathbf{v}^h = \boldsymbol{\Pi}_{\text{algo}}^e : \nabla \mathbf{v}^h + \boldsymbol{\Pi}_{i+\frac{1}{2}}^v : \nabla \mathbf{v}^h$ and $\ddot{\mathbf{u}}_{i+\frac{1}{2}}^{h\Delta t} = \frac{\dot{\mathbf{u}}_{i+1}^{h\Delta t} - \dot{\mathbf{u}}_i^{h\Delta t}}{\Delta t}$ is the approximation of the acceleration $\ddot{\mathbf{u}}$ at time $t_{i+\frac{1}{2}}$. Starting from problem $\mathcal{P}_V^{h\Delta t}$ and using the formalism introduced in [65] based on the Galerkin approximation for hyperelasticity, we will directly pose the strong discrete elementary problem as follows.

Problem $\mathcal{P}_S^{\text{nodal}}$. *Find a global displacement vector* $\mathbf{u}^{\Delta t} = \{\mathbf{u}_i^{\Delta t}\}_{i=0}^n$*, a global scalar normal stress* $\Gamma_{\boldsymbol{\nu}}^{\Delta t} = \{\Gamma_{\boldsymbol{\nu}} i^{\Delta t}\}_{i=0}^n$*, and a global tangential stress vector* $\boldsymbol{\Gamma}_{\boldsymbol{\tau}}^{\Delta t} = \{\boldsymbol{\Gamma}_{\boldsymbol{\tau}} i^{\Delta t}\}_{i=0}^n$ *such that*

$$\rho \ddot{\mathbf{u}}_{i+\frac{1}{2}}^{\Delta t} + A(\mathbf{u}_{i+\frac{1}{2}}^{\Delta t}, \dot{\mathbf{u}}_{i+\frac{1}{2}}^{\Delta t}) + \Gamma_{\boldsymbol{\nu}} {}_{i+\frac{1}{2}}^{\Delta t} \boldsymbol{\nu} + \boldsymbol{\Gamma}_{\boldsymbol{\tau}} {}_{i+\frac{1}{2}}^{\Delta t} - \mathbf{f} - \mathbf{g} = \mathbf{0}, \tag{4.2}$$

where $A(\cdot)$ is the internal force vector stemming from the first Piola–Kirchhoff tensor $\boldsymbol{\Pi}_{\text{algo}}^e$ and the viscous contribution $\boldsymbol{\Pi}^v$. For more details about Problem $\mathcal{P}_S^{\text{nodal}}$ and the operator $A(\cdot)$, we refer the reader to [65, 7, 41].

In the following sections, we propose both Newton's semi-smooth method and the Primal Dual Active Set method algorithm for each case of contact, namely, the law of persistent frictional contact by Coulomb. Thereafter, to simplify notation and readability, we do not indicate the dependence of the variables with respect to the discretization parameters Δt and h. For example, we will write $\mathbf{u}$ instead of $\mathbf{u}_{i+\frac{1}{2}}^{h\Delta t}$.

5. Numerical resolution via a Primal-Dual Active Set method

In this section, we detail the solution of Newton's Semi-smooth method for visco-hyperelastic problems with persistent contact conditions and Coulomb's friction. This method is based on the reformulation of frictional contact conditions in terms of non-linear complementarity equations, whose solution is provided by the Newton semi-smooth iterative method [51, 52, 55]. To this end, we need the generalized derivative of complementary functions for contact and friction. In practice, the conditions of contact with Coulomb's friction can be formulated in terms of a fixed point problem, related to quasi-optimization ones. From a purely algorithmic point of view, the main goal of these methods is to separate the nodes potentially in contact into two subsets (active and inactive) and to find the correct subset of all the nodes actually in active contact (subset $\mathcal{A}$), as opposed to those that are inactive (subset $\mathcal{I}$).
In the following, we specify, among other things, the main principles of Newton's Semi-smooth method such as complementarity functions and their generalized derivatives as well as the PDAS. For further details about the formalism of Newton's Semi-smooth method, see references [51, 52, 55, 53, 54, 41].

5.1. Conditions of persistent frictional contact

We consider a persistent contact law associated with Coulomb's friction law. Denoting by p the index of vertices on $\partial\Omega_c^h \subset \partial\Omega_c$, the discrete persistent conditions verified on the contact boundary $\partial\Omega_c^h$ are given by

$$\begin{aligned} &\text{if } d_{\boldsymbol{\nu},p} > 0: && \Gamma_{\boldsymbol{\nu},p} = 0\ ;\ \mathbf{\Gamma}_{\boldsymbol{\tau},p} = 0 && (5.1)\\ &\text{if } d_{\boldsymbol{\nu},p} = 0: && && \\ & && \overset{\circ}{d}_{\boldsymbol{\nu},p} \geq 0, && (5.2)\\ & && \Gamma_{\boldsymbol{\nu},p} \leq 0, && (5.3)\\ & && \overset{\circ}{d}_{\boldsymbol{\nu},p}\, \Gamma_{\boldsymbol{\nu},p} = 0, && (5.4) \end{aligned}$$

and

$$\begin{cases} \overset{\circ}{\mathbf{d}}_{\boldsymbol{\tau},p} = \|\overset{\circ}{\mathbf{d}}_{\boldsymbol{\tau},p}\| \dfrac{\mathbf{\Gamma}_{\boldsymbol{\tau},p}}{\|\mathbf{\Gamma}_{\boldsymbol{\tau},p}\|}, \\ \|\mathbf{\Gamma}_{\boldsymbol{\tau},p}\| + \mu\Gamma_{\boldsymbol{\nu},p} \leq 0, \\ \|\overset{\circ}{\mathbf{d}}_{\boldsymbol{\tau},p}\|(\|\mathbf{\Gamma}_{\boldsymbol{\tau},p}\| + \mu\Gamma_{\boldsymbol{\nu},p}) = 0. \end{cases} \tag{5.5}$$

5.2. Semi-smooth Newton approach

Contact complementarity function

The first non-linear complementarity function (real-valued function) associated with persistent contact conditions, i.e. with relations (5.2)–(5.4), is

$$\mathcal{R}^{\mathbf{\Gamma}}_{\boldsymbol{\nu}}(\overset{\circ}{d}_{\boldsymbol{\nu},p}, \Gamma_{\boldsymbol{\nu},p}) = -\Gamma_{\boldsymbol{\nu},p} - \max(0, -\Gamma_{\boldsymbol{\nu},p} - c_{\boldsymbol{\nu}}\, \overset{\circ}{d}_{\boldsymbol{\nu},p}). \tag{5.6}$$

Proposition 5.1. *Let $c_{\boldsymbol{\nu}} > 0$, the contact conditions* (5.2)–(5.4) *are equivalent to the relation $\mathcal{R}^{\mathbf{\Gamma}}_{\boldsymbol{\nu}}(\overset{\circ}{d}_{\boldsymbol{\nu},p}, \Gamma_{\boldsymbol{\nu},p}) = 0$.*

Proof. See [57]. □

Frictional contact complementarity function

The second non-linear complementarity function (vector-valued function) associated with the friction conditions, i.e. with the relations equivalent to (5.5), is:

$$\mathcal{R}^{\mathbf{\Gamma}}_{\boldsymbol{\tau}}(\overset{\circ}{d}_{\boldsymbol{\nu},p}, \overset{\circ}{\mathbf{d}}_{\boldsymbol{\tau},p}, \Gamma_{\boldsymbol{\nu},p}, \mathbf{\Gamma}_{\boldsymbol{\tau},p}) = \max(-\mu\Gamma_{\boldsymbol{\nu},p}, \|\mathbf{\Gamma}_{\boldsymbol{\tau},p} + c_{\boldsymbol{\tau}}\, \overset{\circ}{\mathbf{d}}_{\boldsymbol{\tau},p}\|)\mathbf{\Gamma}_{\boldsymbol{\tau},p} + \mu\Gamma_{\boldsymbol{\nu},p}(\mathbf{\Gamma}_{\boldsymbol{\tau},p} + c_{\boldsymbol{\tau}}\, \overset{\circ}{\mathbf{d}}_{\boldsymbol{\tau},p}). \tag{5.7}$$

Proposition 5.2. *Let $c_{\boldsymbol{\tau}} > 0$, Coulomb's friction conditions* (5.5) *are equivalent to the relation*

$$\mathcal{R}^{\mathbf{\Gamma}}_{\boldsymbol{\tau}}(\overset{\circ}{d}_{\boldsymbol{\nu},p}, \overset{\circ}{\mathbf{d}}_{\boldsymbol{\tau},p}, \Gamma_{\boldsymbol{\nu},p}, \mathbf{\Gamma}_{\boldsymbol{\tau},p}) = 0.$$

Proof. See [41]. □

Generalized derivative of complementarity functions

We now give the generalized derivative of the complementarity functions for the cases with no contact **(Gap case)**, sticking **(Stick case)**, and sliding **(Slip case)**.

• Gap case: $\Gamma_{\boldsymbol{\nu},p} + c_{\boldsymbol{\nu}}\overset{\circ}{d}_{\boldsymbol{\nu},p} \geq 0$.

As per relations (5.6) and (5.7), the complementarity functions $\mathcal{R}^{\mathbf{\Gamma}}_{\boldsymbol{\nu}}$ and $\mathcal{R}^{\mathbf{\Gamma}}_{\boldsymbol{\tau}}$ take the form

$$\mathcal{R}^{\mathbf{\Gamma}}_{\boldsymbol{\nu}}(\overset{\circ}{d}_{\boldsymbol{\nu},p}, \Gamma_{\boldsymbol{\nu},p}) = -\Gamma_{\boldsymbol{\nu},p},$$
$$\mathcal{R}^{\mathbf{\Gamma}}_{\boldsymbol{\tau}}(\overset{\circ}{d}_{\boldsymbol{\nu},p}, \overset{\circ}{\mathbf{d}}_{\boldsymbol{\tau},p}, \Gamma_{\boldsymbol{\nu},p}, \mathbf{\Gamma}_{\boldsymbol{\tau},p}) = \|\mathbf{\Gamma}_{\boldsymbol{\tau},p} + c_{\boldsymbol{\tau}}\, \overset{\circ}{\mathbf{d}}_{\boldsymbol{\tau},p}\| \mathbf{\Gamma}_{\boldsymbol{\tau},p}.$$

This results in the following derivatives for $\mathcal{R}^{\mathbf{\Gamma}}_{\boldsymbol{\nu}}$:

$$\mathbb{d}_{\overset{\circ}{d}_{\boldsymbol{\nu},p}} \mathcal{R}^{\mathbf{\Gamma}}_{\boldsymbol{\nu}} = 0, \tag{5.8}$$
$$\mathbb{d}_{\Gamma_{\boldsymbol{\nu},p}} \mathcal{R}^{\mathbf{\Gamma}}_{\boldsymbol{\nu}} = -\mathbb{d}\Gamma_{\boldsymbol{\nu},p}, \tag{5.9}$$

and for $\mathcal{R}^{\mathbf{\Gamma}}_{\boldsymbol{\tau}}$, we have

$$\mathbb{d}_{\overset{\circ}{d}_{\boldsymbol{\nu},p}} \mathcal{R}^{\mathbf{\Gamma}}_{\boldsymbol{\tau}} = 0, \tag{5.10}$$
$$\mathbb{d}_{\overset{\circ}{\mathbf{d}}_{\boldsymbol{\tau},p}} \mathcal{R}^{\mathbf{\Gamma}}_{\boldsymbol{\tau}} = c_{\boldsymbol{\tau}} \mathbf{\Gamma}_{\tau,p} \otimes \frac{\mathbf{\Gamma}_{\boldsymbol{\tau},p} + c_{\boldsymbol{\tau}}\, \overset{\circ}{\mathbf{d}}_{\boldsymbol{\tau},p}}{\|\mathbf{\Gamma}_{\boldsymbol{\tau},p} + c_{\boldsymbol{\tau}}\, \overset{\circ}{\mathbf{d}}_{\boldsymbol{\tau},p}\|} \mathbb{d}\overset{\circ}{\mathbf{d}}_{\boldsymbol{\tau},p} = 0, \tag{5.11}$$
$$\mathbb{d}_{\Gamma_{\boldsymbol{\nu},p}} \mathcal{R}^{\mathbf{\Gamma}}_{\boldsymbol{\tau}} = 0, \tag{5.12}$$
$$\mathbb{d}_{\mathbf{\Gamma}_{\boldsymbol{\tau},p}} \mathcal{R}^{\mathbf{\Gamma}}_{\boldsymbol{\tau}} = \Big(\mathbf{\Gamma}_{\boldsymbol{\tau},p} \otimes \frac{\mathbf{\Gamma}_{\boldsymbol{\tau},p} + c_{\boldsymbol{\tau}}\, \overset{\circ}{\mathbf{d}}_{\boldsymbol{\tau},p}}{\|\mathbf{\Gamma}_{\boldsymbol{\tau},p} + c_{\boldsymbol{\tau}}\, \overset{\circ}{\mathbf{d}}_{\boldsymbol{\tau},p}\|} + \|\mathbf{\Gamma}_{\boldsymbol{\tau},p} + c_{\boldsymbol{\tau}}\, \overset{\circ}{\mathbf{d}}_{\boldsymbol{\tau},p}\| \mathbf{I}_2\Big) \mathbb{d}\mathbf{\Gamma}_{\boldsymbol{\tau},p}. \tag{5.13}$$

• Stick case: $\Gamma_{\boldsymbol{\nu},p} + c_{\boldsymbol{\nu}} \overset{\circ}{d}_{\boldsymbol{\nu},p} < 0$ and $\|\mathbf{\Gamma}_{\boldsymbol{\tau},p} + c_{\boldsymbol{\tau}}\, \overset{\circ}{\mathbf{d}}_{\boldsymbol{\tau},p}\| < -\mu\Gamma_{\boldsymbol{\nu},p}$.

We now get, in this case,

$$\mathcal{R}^{\mathbf{\Gamma}}_{\boldsymbol{\nu}}(\overset{\circ}{d}_{\boldsymbol{\nu},p}, \Gamma_{\boldsymbol{\nu},p}) = c_{\boldsymbol{\nu}}\, \overset{\circ}{d}_{\boldsymbol{\nu},p},$$
$$\mathcal{R}^{\mathbf{\Gamma}}_{\boldsymbol{\tau}}(\overset{\circ}{d}_{\boldsymbol{\nu},p}, \overset{\circ}{\mathbf{d}}_{\boldsymbol{\tau},p}, \Gamma_{\boldsymbol{\nu},p}, \mathbf{\Gamma}_{\boldsymbol{\tau},p}) = \mu c_{\boldsymbol{\tau}} \Gamma_{\boldsymbol{\nu},p}\, \overset{\circ}{\mathbf{d}}_{\boldsymbol{\tau},p}\, .$$

As a result, for $\mathcal{R}^{\mathbf{\Gamma}}_{\boldsymbol{\nu}}$ we get

$$\mathbb{d}_{\overset{\circ}{d}_{\boldsymbol{\nu},p}} \mathcal{R}^{\mathbf{\Gamma}}_{\boldsymbol{\nu}} = c_{\boldsymbol{\nu}}\, \mathbb{d}\overset{\circ}{d}_{\boldsymbol{\nu},p}, \tag{5.14}$$
$$\mathbb{d}_{\Gamma_{\boldsymbol{\nu},p}} \mathcal{R}^{\mathbf{\Gamma}}_{\boldsymbol{\nu}} = 0, \tag{5.15}$$

and for $\mathcal{R}^{\mathbf{\Gamma}}_{\boldsymbol{\tau}}$, we have

$$\mathbb{d}_{\overset{\circ}{d}_{\boldsymbol{\nu},p}} \mathcal{R}^{\mathbf{\Gamma}}_{\boldsymbol{\tau}} = 0, \tag{5.16}$$
$$\mathbb{d}_{\overset{\circ}{\mathbf{d}}_{\boldsymbol{\tau},p}} \mathcal{R}^{\mathbf{\Gamma}}_{\boldsymbol{\tau}} = \mu c_{\boldsymbol{\tau}} \Gamma_{\boldsymbol{\nu},p} \mathbb{d}\, \overset{\circ}{\mathbf{d}}_{\boldsymbol{\tau},p}, \tag{5.17}$$
$$\mathbb{d}_{\Gamma_{\boldsymbol{\nu},p}} \mathcal{R}^{\mathbf{\Gamma}}_{\boldsymbol{\tau}} = \mu c_{\boldsymbol{\tau}}\, \overset{\circ}{\mathbf{d}}_{\boldsymbol{\tau},p}\, \mathbb{d}\Gamma_{\boldsymbol{\nu},p}, \tag{5.18}$$
$$\mathbb{d}_{\mathbf{\Gamma}_{\boldsymbol{\tau},p}} \mathcal{R}^{\mathbf{\Gamma}}_{\boldsymbol{\tau}} = 0. \tag{5.19}$$

• Slip case: $\Gamma_{\boldsymbol{\nu},p} + c_{\boldsymbol{\nu}} \overset{\circ}{d}_{\boldsymbol{\nu},p} < 0$ and $-\mu\Gamma_{\boldsymbol{\nu},p} \leq \|\mathbf{\Gamma}_{\boldsymbol{\tau},p} + c_{\boldsymbol{\tau}}\, \overset{\circ}{\mathbf{d}}_{\boldsymbol{\tau},p}\|$.

Finally, the relations (5.6) and (5.7) give

$$\mathcal{R}^{\mathbf{\Gamma}}_{\boldsymbol{\nu}}(\overset{\circ}{d}_{\boldsymbol{\nu},p}, \Gamma_{\boldsymbol{\nu},p}) = c_{\boldsymbol{\nu}}\, \overset{\circ}{d}_{\boldsymbol{\nu},p},$$
$$\mathcal{R}^{\mathbf{\Gamma}}_{\boldsymbol{\tau}}(\overset{\circ}{d}_{\boldsymbol{\nu},p}, \overset{\circ}{\mathbf{d}}_{\boldsymbol{\tau},p}, \Gamma_{\boldsymbol{\nu},p}, \mathbf{\Gamma}_{\boldsymbol{\tau},p}) = \|\mathbf{\Gamma}_{\boldsymbol{\tau},p} + c_{\boldsymbol{\tau}}\, \overset{o}{\mathbf{d}}_{\boldsymbol{\tau},p}\| \mathbf{\Gamma}_{\boldsymbol{\tau},p} + \mu\Gamma_{\boldsymbol{\nu},p}(\mathbf{\Gamma}_{\boldsymbol{\tau},p} + c_{\boldsymbol{\tau}}\, \overset{\circ}{\mathbf{d}}_{\boldsymbol{\tau},p}).$$

We obtain the following derivatives for $\mathcal{R}^{\mathbf{\Gamma}}_{\boldsymbol{\nu}}$

$$\mathbb{d}_{\substack{\circ \\ d_{\boldsymbol{\nu},p}}} \mathcal{R}^{\mathbf{\Gamma}}_{\boldsymbol{\nu}} = c_{\boldsymbol{\nu}}\, \mathbb{d}\overset{\circ}{d}_{\boldsymbol{\nu},p}, \tag{5.20}$$

$$\mathbb{d}_{\Gamma_{\boldsymbol{\nu},p}} \mathcal{R}^{\mathbf{\Gamma}}_{\boldsymbol{\nu}} = 0, \tag{5.21}$$

and for $\mathcal{R}^{\mathbf{\Gamma}}_{\boldsymbol{\tau}}$, we have

$$\mathbb{d}_{\substack{\circ \\ d_{\boldsymbol{\nu},p}}} \mathcal{R}^{\mathbf{\Gamma}}_{\boldsymbol{\tau}} = 0, \tag{5.22}$$

$$\mathbb{d}_{\substack{\circ \\ \mathbf{d}_{\boldsymbol{\tau},p}}} \mathcal{R}^{\mathbf{\Gamma}}_{\boldsymbol{\tau}} = \Big(c_{\boldsymbol{\tau}} \mathbf{\Gamma}_{\boldsymbol{\tau},p} \otimes \frac{\mathbf{\Gamma}_{\boldsymbol{\tau},p} + c_{\boldsymbol{\tau}}\, \overset{\circ}{\mathbf{d}}_{\boldsymbol{\tau},p}}{\|\mathbf{\Gamma}_{\boldsymbol{\tau},p} + c_{\boldsymbol{\tau}}\, \overset{\circ}{\mathbf{d}}_{\boldsymbol{\tau},p}\|} + \mu c_{\boldsymbol{\tau}} \Gamma_{\boldsymbol{\nu},p} \mathbf{I}_2\Big) \mathbb{d}\overset{\circ}{\mathbf{d}}_{\boldsymbol{\tau},p}, \tag{5.23}$$

$$\mathbb{d}_{\Gamma_{\boldsymbol{\nu},p}} \mathcal{R}^{\mathbf{\Gamma}}_{\boldsymbol{\tau}} = \mu(\mathbf{\Gamma}_{\boldsymbol{\tau},p} + c_{\boldsymbol{\tau}}\, \overset{\circ}{\mathbf{d}}_{\boldsymbol{\tau},p}) \mathbb{d}\Gamma_{\boldsymbol{\nu},p}, \tag{5.24}$$

$$\mathbb{d}_{\mathbf{\Gamma}_{\boldsymbol{\tau},p}} \mathcal{R}^{\mathbf{\Gamma}}_{\boldsymbol{\tau}} = \Big(\mathbf{\Gamma}_{\boldsymbol{\tau},p} \otimes \frac{\mathbf{\Gamma}_{\boldsymbol{\tau},p} + c_{\boldsymbol{\tau}}\, \overset{\circ}{\mathbf{d}}_{\boldsymbol{\tau},p}}{\|\mathbf{\Gamma}_{\boldsymbol{\tau},p} + c_{\boldsymbol{\tau}}\, \overset{\circ}{\mathbf{d}}_{\boldsymbol{\tau},p}\|} + \|\mathbf{\Gamma}_{\boldsymbol{\tau},p} + c_{\boldsymbol{\tau}}\, \overset{\circ}{\mathbf{d}}_{\boldsymbol{\tau},p}\| \mathbf{I}_2 + \mu \Gamma_{\boldsymbol{\nu},p} \mathbf{I}_2\Big) \mathbb{d}\mathbf{\Gamma}_{\boldsymbol{\tau},p}. \tag{5.25}$$

By combining (5.8)–(5.25), denoting by $\mathcal{G}_{\mathcal{R}^{\mathbf{\Gamma}}_{\boldsymbol{\nu}}}$ and $\mathcal{G}_{\mathcal{R}^{\mathbf{\Gamma}}_{\boldsymbol{\tau}}}$ the generalized derivatives of $\mathcal{R}^{\mathbf{\Gamma}}_{\boldsymbol{\nu}}$ and $\mathcal{R}^{\mathbf{\Gamma}}_{\boldsymbol{\tau}}$, we get respectively

$$\mathcal{G}_{\mathcal{R}^{\mathbf{\Gamma}}_{\boldsymbol{\nu}}}(\overset{\circ}{d}_{\boldsymbol{\nu},p}, \Gamma_{\boldsymbol{\nu},p})(\delta\, \overset{\circ}{d}_{\boldsymbol{\nu},p}, \delta\Gamma_{\boldsymbol{\nu},p}) = c_{\boldsymbol{\nu}}(\mathcal{X}_{\text{Stick}} + \mathcal{X}_{\text{Slip}})\, \delta\, \overset{\circ}{d}_{\boldsymbol{\nu},p} + \mathcal{X}_{\text{Gap}} \delta\Gamma_{\boldsymbol{\nu},p}, \tag{5.26}$$

$$\begin{aligned}
\mathcal{G}_{\mathcal{R}^{\mathbf{\Gamma}}_{\boldsymbol{\tau}}}(\overset{\circ}{d}_{\boldsymbol{\nu},p}, \overset{\circ}{\mathbf{d}}_{\boldsymbol{\tau},p}, \Gamma_{\boldsymbol{\nu},p}, \mathbf{\Gamma}_{\boldsymbol{\tau},p})(\delta\, \overset{\circ}{d}_{\boldsymbol{\nu},p}, \delta\, \overset{\circ}{\mathbf{d}}_{\boldsymbol{\tau},p}, \delta\Gamma_{\boldsymbol{\nu},p}, \delta\mathbf{\Gamma}_{\boldsymbol{\tau},p}) &= \mathcal{X}_{\text{Gap}} \|\mathbf{\Gamma}_{\boldsymbol{\tau},p} + c_{\boldsymbol{\tau}}\, \overset{\circ}{\mathbf{d}}_{\boldsymbol{\tau},p}\| \delta\mathbf{\Gamma}_{\boldsymbol{\tau},p} \\
&+ \mathcal{X}_{\text{Stick}} \Big(\mu c_{\boldsymbol{\tau}} \Gamma_{\boldsymbol{\nu},p} \delta\, \overset{\circ}{\mathbf{d}}_{\boldsymbol{\tau},p} + \mu c_{\boldsymbol{\tau}}\, \overset{\circ}{\mathbf{d}}_{\boldsymbol{\tau},p}\, \delta\Gamma_{\boldsymbol{\nu},p}\Big) \\
&+ \mathcal{X}_{\text{Slip}} \Big(\Big(c_{\boldsymbol{\tau}} \mathbf{\Gamma}_{\boldsymbol{\tau},p} \otimes \frac{(\mathbf{\Gamma}_{\boldsymbol{\tau},p} + c_{\boldsymbol{\tau}}\, \overset{\circ}{\mathbf{d}}_{\boldsymbol{\tau},p})}{\|\mathbf{\Gamma}_{\boldsymbol{\tau},p} + c_{\boldsymbol{\tau}}\, \overset{\circ}{\mathbf{d}}_{\boldsymbol{\tau},p}\|} + \mu c_{\boldsymbol{\tau}} \Gamma_{\boldsymbol{\nu},p} \mathbf{I}_2\Big) \delta\overset{\circ}{\mathbf{d}}_{\tau,p} + \mu(\mathbf{\Gamma}_{\boldsymbol{\tau},p} + c_{\boldsymbol{\tau}}\, \overset{\circ}{\mathbf{d}}_{\boldsymbol{\tau},p}) \delta\Gamma_{\nu,p} \\
&+ \Big(\mathbf{\Gamma}_{\boldsymbol{\tau},p} \otimes \frac{(\mathbf{\Gamma}_{\boldsymbol{\tau},p} + c_{\boldsymbol{\tau}}\, \overset{\circ}{\mathbf{d}}_{\boldsymbol{\tau},p})}{\|\mathbf{\Gamma}_{\boldsymbol{\tau},p} + c_{\boldsymbol{\tau}}\, \overset{\circ}{\mathbf{d}}_{\boldsymbol{\tau},p}\|} + \|\mathbf{\Gamma}_{\boldsymbol{\tau},p} + c_{\boldsymbol{\tau}}\, \overset{\circ}{\mathbf{d}}_{\boldsymbol{\tau},p}\| \mathbf{I}_2 + \mu \Gamma_{\boldsymbol{\nu},p} \mathbf{I}_2\Big) \delta\mathbf{\Gamma}_{\boldsymbol{\tau},p}\Big),
\end{aligned} \tag{5.27}$$

where

$$\begin{aligned}
&\mathcal{X}_{\text{Gap}} = 1,\ \mathcal{X}_{\text{Stick}} = 0,\ \mathcal{X}_{\text{Slip}} = 0 \text{ if } \ \Gamma_{\boldsymbol{\nu},p} + c_{\boldsymbol{\nu}}\, \overset{\circ}{d}_{\boldsymbol{\nu},p} \geq 0, \\
&\mathcal{X}_{\text{Gap}} = 0,\ \mathcal{X}_{\text{Stick}} = 1,\ \mathcal{X}_{\text{Slip}} = 0 \text{ if } \ \|\mathbf{\Gamma}_{\boldsymbol{\tau},p} + c_{\boldsymbol{\tau}}\, \overset{\circ}{\mathbf{d}}_{\boldsymbol{\tau},p}\| < -\mu\Gamma_{\boldsymbol{\nu},p}, \\
&\mathcal{X}_{\text{Gap}} = 0,\ \mathcal{X}_{\text{Stick}} = 0,\ \mathcal{X}_{\text{Slip}} = 1 \text{ if } \ -\mu\Gamma_{\boldsymbol{\nu},p} \leq \|\mathbf{\Gamma}_{\boldsymbol{\tau},p} + c_{\boldsymbol{\tau}}\, \overset{\circ}{\mathbf{d}}_{\boldsymbol{\tau},p}\|.
\end{aligned}$$

Now using Newton's semi-smooth formalism (indexed by superscript k) on the current fixed point $(\overset{\circ(k)}{d}_{\boldsymbol{\nu},p}, \overset{\circ(k)}{\mathbf{d}}_{\boldsymbol{\tau},p}, \Gamma^{(k)}_{\boldsymbol{\nu},p}, \mathbf{\Gamma}^{(k)}_{\boldsymbol{\tau},p})$ from generalized derivatives (5.26) and (5.27), we can deduce the new iterated list $(\overset{\circ(k+1)}{d}_{\boldsymbol{\nu},p}, \overset{\circ(k+1)}{\mathbf{d}}_{\boldsymbol{\tau},p}, \Gamma^{(k+1)}_{\boldsymbol{\nu},p}, \mathbf{\Gamma}^{(k+1)}_{\boldsymbol{\tau},p})$ with the following iterative scheme of index $(k+1)$:

$$\mathcal{G}_{\mathcal{R}^{\mathbf{\Gamma}}_{\boldsymbol{\nu}}}(\overset{\circ(k)}{d}_{\boldsymbol{\nu},p}, \Gamma^{(k)}_{\boldsymbol{\nu},p})(\delta\, \overset{\circ(k+1)}{d}_{\boldsymbol{\nu},p}, \delta\Gamma^{(k+1)}_{\boldsymbol{\nu},p}) = -\mathcal{R}^{\mathbf{\Gamma}}_{\boldsymbol{\nu}}(\overset{\circ(k)}{d}_{\boldsymbol{\nu},p}, \Gamma^{(k)}_{\boldsymbol{\nu},p}),$$

$$\mathcal{G}_{\mathcal{R}^{\mathbf{\Gamma}}_{\boldsymbol{\tau}}}(\overset{\circ(k)}{d}_{\boldsymbol{\nu},p}, \overset{\circ(k)}{\mathbf{d}}_{\boldsymbol{\tau},p}, \Gamma^{(k)}_{\boldsymbol{\nu},p}, \mathbf{\Gamma}^{(k)}_{\boldsymbol{\tau},p})(\delta\, \overset{\circ(k+1)}{d}_{\boldsymbol{\nu},p}, \delta\, \overset{\circ(k+1)}{\mathbf{d}}_{\tau,p}, \delta\Gamma^{(k+1)}_{\boldsymbol{\nu},p}, \delta\mathbf{\Gamma}^{(k+1)}_{\boldsymbol{\tau},p}) = -\mathcal{R}^{\mathbf{\Gamma}}_{\boldsymbol{\tau}}(\overset{\circ(k)}{d}_{\boldsymbol{\nu},p}, \overset{\circ(k)}{\mathbf{d}}_{\boldsymbol{\tau},p}, \Gamma^{(k)}_{\boldsymbol{\nu},p}, \mathbf{\Gamma}^{(k)}_{\boldsymbol{\tau},p}),$$

$$(\overset{\circ(k+1)}{d}_{\boldsymbol{\nu},p}, \overset{\circ(k+1)}{\mathbf{d}}_{\boldsymbol{\tau},p}, \Gamma^{(k+1)}_{\boldsymbol{\nu},p}, \mathbf{\Gamma}^{(k+1)}_{\boldsymbol{\tau},p}) = (\overset{\circ(k)}{d}_{\boldsymbol{\nu},p}, \overset{\circ(k)}{\mathbf{d}}_{\boldsymbol{\tau},p}, \Gamma^{(k)}_{\boldsymbol{\nu},p}, \mathbf{\Gamma}^{(k)}_{\boldsymbol{\tau},p}) + (\delta\, \overset{\circ(k+1)}{d}_{\boldsymbol{\nu},p}, \delta\, \overset{\circ(k+1)}{\mathbf{d}}_{\boldsymbol{\tau},p}, \delta\Gamma^{(k+1)}_{\boldsymbol{\nu},p}, \delta\mathbf{\Gamma}^{(k+1)}_{\boldsymbol{\tau},p}).$$

where $\delta\square^{(k+1)} = \square^{(k+1)} - \square^{(k)}$.
According to the different cases of contact state (no-contact, sticking, and sliding), and applying the previous derivatives in Newton's semi-smooth formalism, we obtain the following cases.

• Gap case: $\mathcal{X}_{\text{Gap}} = 1, \mathcal{X}_{\text{Stick}} = 0, \mathcal{X}_{\text{Slip}} = 0.$

We have

$$-(\Gamma_{\boldsymbol{\nu},p}^{(k+1)} - \Gamma_{\boldsymbol{\nu},p}^{(k)}) = \Gamma_{\boldsymbol{\nu},p}^{(k)} \quad \text{and} \quad \|\boldsymbol{\Gamma}_{\boldsymbol{\tau},p}^{(k)} + c_{\boldsymbol{\tau}} \overset{\circ}{\mathbf{d}}{}_{\boldsymbol{\tau},p}^{(k)}\|(\boldsymbol{\Gamma}_{\boldsymbol{\tau},p}^{(k+1)} - \boldsymbol{\Gamma}_{\boldsymbol{\tau},p}^{(k)}) = -\|\boldsymbol{\Gamma}_{\boldsymbol{\tau},p}^{(k)} + c_{\boldsymbol{\tau}} \overset{\circ}{\mathbf{d}}{}_{\boldsymbol{\tau},p}^{(k)}\|\boldsymbol{\Gamma}_{\boldsymbol{\tau},p}^{(k)}. \tag{5.28}$$

It follows

$$\Gamma_{\boldsymbol{\nu},p}^{(k+1)} = 0 \quad \text{and} \quad \boldsymbol{\Gamma}_{\boldsymbol{\tau},p}^{(k+1)} = 0, \tag{5.29}$$

since $\|\boldsymbol{\Gamma}_{\boldsymbol{\tau},p}^{(k)} + c_{\boldsymbol{\tau}} \overset{\circ}{\mathbf{d}}{}_{\boldsymbol{\tau},p}^{(k)}\| > 0$.

• Stick case: $\mathcal{X}_{\text{Gap}} = 0, \mathcal{X}_{\text{Stick}} = 1, \mathcal{X}_{\text{Slip}} = 0.$

We have

$$c_{\boldsymbol{\nu}}(\overset{\circ}{d}{}_{\boldsymbol{\nu},p}^{(k+1)} - \overset{\circ}{d}{}_{\boldsymbol{\nu},p}^{(k)}) = -c_{\boldsymbol{\nu}} \overset{\circ}{d}{}_{\boldsymbol{\nu},p}^{(k)} \quad \text{and} \quad \mu c_{\boldsymbol{\tau}} \Gamma_{\boldsymbol{\nu},p}^{(k)}(\overset{\circ}{\mathbf{d}}{}_{\boldsymbol{\tau},p}^{(k+1)} - \overset{\circ}{\mathbf{d}}{}_{\boldsymbol{\tau},p}^{(k)}) + \mu c_{\boldsymbol{\tau}} \overset{\circ}{\mathbf{d}}{}_{\boldsymbol{\tau},p}^{(k)} (\Gamma_{\boldsymbol{\nu},p}^{(k+1)} - \Gamma_{\boldsymbol{\nu},p}^{(k)}) = -\mu c_{\boldsymbol{\tau}} \Gamma_{\boldsymbol{\nu},p}^{(k)} \overset{\circ}{\mathbf{d}}{}_{\boldsymbol{\tau},p}^{(k)}, \tag{5.30}$$

whence

$$\overset{\circ}{d}{}_{\boldsymbol{\nu},p}^{(k+1)} = 0 \quad \text{and} \quad \overset{\circ}{\mathbf{d}}{}_{\boldsymbol{\tau},p}^{(k+1)} + \frac{\overset{\circ}{\mathbf{d}}{}_{\boldsymbol{\tau},p}^{(k)}}{\Gamma_{\boldsymbol{\nu},p}^{(k)}} \Gamma_{\boldsymbol{\nu},p}^{(k+1)} = \overset{\circ}{\mathbf{d}}{}_{\tau,p}^{(k)}. \tag{5.31}$$

• Slip case: $\mathcal{X}_{\text{Gap}} = 0, \mathcal{X}_{\text{Stick}} = 0, \mathcal{X}_{\text{Slip}} = 1.$

For $\mathcal{R}_{\boldsymbol{\nu}}^{\boldsymbol{\Gamma}}$, we get again

$$\overset{\circ}{d}{}_{\boldsymbol{\nu},p}^{(k+1)} = 0 \tag{5.32}$$

For $\mathcal{R}_{\boldsymbol{\tau}}^{\boldsymbol{\Gamma}}$, we get

$$\begin{aligned}
&\Big(c_{\boldsymbol{\tau}} \boldsymbol{\Gamma}_{\boldsymbol{\tau},p}^{(k)} \otimes \frac{\boldsymbol{\Gamma}_{\boldsymbol{\tau},p}^{(k)} + c_{\boldsymbol{\tau}} \overset{\circ}{\mathbf{d}}{}_{\boldsymbol{\tau},p}^{(k)}}{\|\boldsymbol{\Gamma}_{\boldsymbol{\tau},p}^{(k)} + c_{\boldsymbol{\tau}} \overset{\circ}{\mathbf{d}}{}_{\boldsymbol{\tau},p}^{(k)}\|} + \mu c_{\boldsymbol{\tau}} \Gamma_{\boldsymbol{\nu},p}^{(k)} \mathbf{I}_2\Big)(\overset{\circ}{\mathbf{d}}{}_{\boldsymbol{\tau},p}^{(k+1)} - \overset{\circ}{\mathbf{d}}{}_{\boldsymbol{\tau},p}^{(k)}) + \mu(\boldsymbol{\Gamma}_{\boldsymbol{\tau},p}^{(k)} + c_{\boldsymbol{\tau}} \overset{\circ}{\mathbf{d}}{}_{\boldsymbol{\tau},p}^{(k)})(\Gamma_{\boldsymbol{\nu},p}^{(k+1)} - \Gamma_{\boldsymbol{\nu},p}^{(k)}) \\
&+ \Big(\boldsymbol{\Gamma}_{\boldsymbol{\tau},p}^{(k)} \otimes \frac{\boldsymbol{\Gamma}_{\boldsymbol{\tau},p}^{(k)} + c_{\boldsymbol{\tau}} \overset{\circ}{\mathbf{d}}{}_{\boldsymbol{\tau},p}^{(k)}}{\|\boldsymbol{\Gamma}_{\boldsymbol{\tau},p}^{(k)} + c_{\boldsymbol{\tau}} \overset{\circ}{\mathbf{d}}{}_{\boldsymbol{\tau},p}^{(k)}\|} + \|\boldsymbol{\Gamma}_{\boldsymbol{\tau},p}^{(k)} + c_{\boldsymbol{\tau}} \overset{\circ}{\mathbf{d}}{}_{\boldsymbol{\tau},p}^{(k)}\|\mathbf{I}_2 + \mu\Gamma_{\boldsymbol{\nu},p}^{(k)} \mathbf{I}_2\Big)(\boldsymbol{\Gamma}_{\boldsymbol{\tau},p}^{(k+1)} - \boldsymbol{\Gamma}_{\boldsymbol{\tau},p}^{(k)}) \\
&\quad = -\|\boldsymbol{\Gamma}_{\boldsymbol{\tau},p}^{(k)} + c_{\boldsymbol{\tau}} \overset{\circ}{\mathbf{d}}{}_{\boldsymbol{\tau},p}^{(k)}\|\boldsymbol{\Gamma}_{\boldsymbol{\tau},p}^{(k)} - \mu\Gamma_{\boldsymbol{\nu},p}^{(k)}(\boldsymbol{\Gamma}_{\boldsymbol{\tau},p}^{(k)} + c_{\boldsymbol{\tau}} \overset{\circ}{\mathbf{d}}{}_{\boldsymbol{\tau},p}^{(k)}).
\end{aligned} \tag{5.33}$$

For a two-dimensional case, we can obtain a simplified equivalent version of the algorithm. Let $\mathcal{G}_{\mathcal{R}_{\boldsymbol{\tau}}^{\boldsymbol{\Gamma}}}^{\text{slip}}$ be the generalized derivative of $\mathcal{R}_{\boldsymbol{\tau}}^{\boldsymbol{\Gamma}}$ in the case with sliding

$$\begin{aligned}
\mathcal{G}_{\mathcal{R}_{\boldsymbol{\tau}}^{\boldsymbol{\Gamma}}}^{\text{slip}}(\overset{\circ}{\mathbf{d}}{}_{\boldsymbol{\tau},p}, \boldsymbol{\Gamma}_{\boldsymbol{\tau},p})(\delta \overset{\circ}{\mathbf{d}}{}_{\boldsymbol{\tau},p}, \delta\boldsymbol{\Gamma}_{\boldsymbol{\tau},p}) &= \boldsymbol{\Gamma}_{\boldsymbol{\tau},p} \otimes \frac{\boldsymbol{\Gamma}_{\boldsymbol{\tau},p} + c_{\boldsymbol{\tau}} \overset{\circ}{\mathbf{d}}{}_{\boldsymbol{\tau},p}}{\|\boldsymbol{\Gamma}_{\boldsymbol{\tau},p} + c_{\boldsymbol{\tau}} \overset{\circ}{\mathbf{d}}{}_{\boldsymbol{\tau},p}\|}(\delta\boldsymbol{\Gamma}_{\boldsymbol{\tau},p} + c_{\boldsymbol{\tau}} \delta \overset{\circ}{\mathbf{d}}{}_{\boldsymbol{\tau},p}) \\
&\quad + \mu\Gamma_{\boldsymbol{\nu},p}(\delta\boldsymbol{\Gamma}_{\boldsymbol{\tau},p} + c_{\boldsymbol{\tau}} \delta \overset{\circ}{\mathbf{d}}{}_{\boldsymbol{\tau},p}) + \mu(\boldsymbol{\Gamma}_{\boldsymbol{\tau},p} + c_{\boldsymbol{\tau}} \overset{\circ}{\mathbf{d}}{}_{\boldsymbol{\tau},p})\delta\Gamma_{\boldsymbol{\nu}} + \|\boldsymbol{\Gamma}_{\boldsymbol{\tau},p} + c_{\boldsymbol{\tau}} \overset{\circ}{\mathbf{d}}{}_{\boldsymbol{\tau},p}\|\delta\boldsymbol{\Gamma}_{\boldsymbol{\tau},p}.
\end{aligned} \tag{5.34}$$

Let $\boldsymbol{\tau}$ be the unit tangential slip vector; since the problem is in contact, we have on the contact boundary

$$\boldsymbol{\Gamma}_{\boldsymbol{\tau},p} = -\mu\Gamma_{\boldsymbol{\nu},p}\boldsymbol{\tau}, \quad \frac{\boldsymbol{\Gamma}_{\boldsymbol{\tau},p} + c_{\boldsymbol{\tau}}\,\overset{\circ}{\mathbf{d}}_{\boldsymbol{\tau},p}}{\|\boldsymbol{\Gamma}_{\boldsymbol{\tau},p} + c_{\boldsymbol{\tau}}\,\overset{\circ}{\mathbf{d}}_{\boldsymbol{\tau},p}\|} = \boldsymbol{\tau}, \quad \delta\boldsymbol{\Gamma}_{\boldsymbol{\tau},p} + c_{\boldsymbol{\tau}}\delta\,\overset{\circ}{\mathbf{d}}_{\boldsymbol{\tau},p} = \alpha\boldsymbol{\tau}, \tag{5.35}$$

for some $\alpha \in \mathbb{R}$. By combining the relations (5.34)–(5.35), we get

$$\mathcal{G}^{\text{slip}}_{\mathcal{R}^{\boldsymbol{\Gamma}}_{\boldsymbol{\tau}}}(\overset{\circ}{\mathbf{d}}_{\boldsymbol{\tau},p}, \boldsymbol{\Gamma}_{\boldsymbol{\tau},p})(\delta\,\overset{\circ}{\mathbf{d}}_{\boldsymbol{\tau},p}, \delta\boldsymbol{\Gamma}_{\boldsymbol{\tau},p}) = -\mu\Gamma_{\boldsymbol{\nu},p}\alpha(\boldsymbol{\tau}\otimes\boldsymbol{\tau} - \mathbf{I}_2)\boldsymbol{\tau} + \mu(\boldsymbol{\Gamma}_{\boldsymbol{\tau},p} + c_{\boldsymbol{\tau}}\,\overset{\circ}{\mathbf{d}}_{\boldsymbol{\tau},p})\delta\Gamma_{\boldsymbol{\nu}} + \|\boldsymbol{\Gamma}_{\boldsymbol{\tau},p} + c_{\boldsymbol{\tau}}\,\overset{o}{\mathbf{d}}_{\boldsymbol{\tau},p}\|\delta\boldsymbol{\Gamma}_{\boldsymbol{\tau},p}.$$

Since $\boldsymbol{\nu}$ and $\boldsymbol{\tau}$ are unit orthogonal vectors, we have in the 2D case $(\boldsymbol{\tau}\otimes\boldsymbol{\tau} - \mathbf{I}_2)\boldsymbol{\tau} = -(\boldsymbol{\nu}\otimes\boldsymbol{\nu})\boldsymbol{\tau} = \mathbf{0}$. Using (5.35) and assuming $\Gamma^{(k)}_{\boldsymbol{\tau}} = -\mu\Gamma^{(k)}_{\boldsymbol{\nu}}\boldsymbol{\tau}^{(k)}$, we deduce from (5.33) the following expression

$$\begin{aligned}\mu(\boldsymbol{\Gamma}^{(k)}_{\boldsymbol{\tau},p} + c_{\boldsymbol{\tau}}\,\overset{\circ(k)}{\mathbf{d}}_{\boldsymbol{\tau},p})(\Gamma^{(k+1)}_{\boldsymbol{\nu},p} - \Gamma^{(k)}_{\boldsymbol{\nu},p}) + \|\boldsymbol{\Gamma}^{(k)}_{\boldsymbol{\tau},p} + c_{\boldsymbol{\tau}}\,\overset{\circ(k)}{\mathbf{d}}_{\boldsymbol{\tau},p}\|(\Gamma^{(k+1)}_{\boldsymbol{\tau},p} - \Gamma^{(k)}_{\boldsymbol{\tau},p}) \\ = -\|\boldsymbol{\Gamma}^{(k)}_{\boldsymbol{\tau},p} + c_{\boldsymbol{\tau}}\,\overset{\circ(k)}{\mathbf{d}}_{\boldsymbol{\tau},p}\|\boldsymbol{\Gamma}^{(k)}_{\boldsymbol{\tau},p} - \mu\Gamma^{(k)}_{\boldsymbol{\nu},p}(\boldsymbol{\Gamma}^{(k)}_{\boldsymbol{\tau},p} + c_{\boldsymbol{\tau}}\,\overset{\circ(k)}{\mathbf{d}}_{\boldsymbol{\tau},p}).\end{aligned} \tag{5.36}$$

Therefore, with elementary algebra, we get

$$\boldsymbol{\Gamma}^{(k+1)}_{\boldsymbol{\tau},p} = -\mu\Gamma^{(k+1)}_{\boldsymbol{\nu},p}\frac{\boldsymbol{\Gamma}^{(k)}_{\boldsymbol{\tau},p} + c_{\boldsymbol{\tau}}\,\overset{\circ(k)}{\mathbf{d}}_{\boldsymbol{\tau},p}}{\|\boldsymbol{\Gamma}^{(k)}_{\boldsymbol{\tau},p} + c_{\boldsymbol{\tau}}\,\overset{\circ(k)}{\mathbf{d}}_{\boldsymbol{\tau},p}\|} = -\mu\Gamma^{(k+1)}_{\boldsymbol{\nu},p}\boldsymbol{\tau}^{(k)}.$$

5.3. Primal-Dual Active Set method

Let $\mathcal{S}$ be the set of all the nodes of the finite element mesh belonging to $\partial\Omega^h_c$ and p the index of a node belonging to $\mathcal{S}$. The discrete frictional contact condition (5.1)–(5.5) is achieved by applying an Active Set strategy on the non-linear complementarity functions $\mathcal{R}^{\boldsymbol{\Gamma}}_{\boldsymbol{\nu}}$ and $\mathcal{R}^{\boldsymbol{\Gamma}}_{\boldsymbol{\tau}}$ based on an iterative semi-smooth Newton procedure. Active and inactive sets for contact and friction are defined according to a leapfrog midpoint scheme as follows:

$$\begin{aligned}\mathcal{A}^{k+1}_{\boldsymbol{\nu}} &= \{p \in \mathcal{S} : \Gamma^{(k)}_{\boldsymbol{\nu},p} + c_{\boldsymbol{\nu}}\,\overset{\circ(k)}{\mathbf{d}}_{\boldsymbol{\nu},p} < 0\},\\ \mathcal{I}^{k+1}_{\boldsymbol{\nu}} &= \{p \in \mathcal{S} : \Gamma^{(k)}_{\boldsymbol{\nu},p} + c_{\boldsymbol{\nu}}\,\overset{\circ(k)}{\mathbf{d}}_{\boldsymbol{\nu},p} \geq 0\},\\ \mathcal{A}^{k+1}_{\boldsymbol{\tau}} &= \{p \in \mathcal{S} : \|\boldsymbol{\Gamma}^{(k)}_{\boldsymbol{\tau},p} + c_{\boldsymbol{\tau}}\,\overset{\circ(k)}{\mathbf{d}}_{\boldsymbol{\tau},p}\| + \mu\Gamma^{(k)}_{\boldsymbol{\nu},p} \geq 0\},\\ \mathcal{I}^{k+1}_{\boldsymbol{\tau}} &= \{p \in \mathcal{S} : \|\boldsymbol{\Gamma}^{(k)}_{\boldsymbol{\tau},p} + c_{\boldsymbol{\tau}}\,\overset{\circ(k)}{\mathbf{d}}_{\boldsymbol{\tau},p}\| + \mu\Gamma^{(k)}_{\boldsymbol{\nu},p} < 0\}.\end{aligned}$$

The status of a node given at iteration k depends on the set to which it belongs; it can either be in the inactive contact state (no-contact state), or in the active contact state (contact state) (see Proposition 5.1) with slip contact or with stick contact. At each time step increment $t_{p+\frac{1}{2}}$, we also introduce $\mathcal{R}(\cdot,\cdot) = \big(\mathcal{R}^{\mathbf{u}}(\cdot,\cdot), \mathcal{R}^{\boldsymbol{\Gamma}}_{\boldsymbol{\nu}}(\cdot,\cdot), \mathcal{R}^{\boldsymbol{\Gamma}}_{\boldsymbol{\tau}}(\cdot,\cdot)\big)$ which describes the system of non-linear equations resulting from the discretized problem $\mathcal{P}^{\text{nodal}}_S$ in the case of unilateral contact with Coulomb's friction, defined by

$$\mathcal{R}(\overset{\circ}{\mathbf{d}}, \boldsymbol{\Gamma}) = \left(\begin{array}{c} \mathcal{R}^{\mathbf{u}}(\overset{\circ}{\mathbf{d}}, \boldsymbol{\Gamma}) = \rho\ddot{\mathbf{u}} + A(\mathbf{u}, \dot{\mathbf{u}}) + \Gamma_{\boldsymbol{\nu}}\boldsymbol{\nu} + \boldsymbol{\Gamma}_{\boldsymbol{\tau}} - \mathbf{f} - \mathbf{g} \\ \mathcal{R}^{\boldsymbol{\Gamma}}_{\boldsymbol{\nu}}(\overset{\circ}{\mathbf{d}}, \boldsymbol{\Gamma}) = -\Gamma_{\boldsymbol{\nu},p} - \max(0, -\Gamma_{\boldsymbol{\nu},p} - c_{\boldsymbol{\nu}}\,\overset{\circ}{d}_{\boldsymbol{\nu},p}) \\ \mathcal{R}^{\boldsymbol{\Gamma}}_{\boldsymbol{\tau}}(\overset{\circ}{\mathbf{d}}, \boldsymbol{\Gamma}) = \max(-\mu\Gamma_{\boldsymbol{\nu},p}, \|\boldsymbol{\Gamma}_{\boldsymbol{\tau},p} + c_{\boldsymbol{\tau}}\,\overset{\circ}{\mathbf{d}}_{\boldsymbol{\tau},p}\|)\boldsymbol{\Gamma}_{\boldsymbol{\tau},p} + \mu\Gamma_{\boldsymbol{\nu},p}(\boldsymbol{\Gamma}_{\boldsymbol{\tau},p} + c_{\boldsymbol{\tau}}\,\overset{\circ}{\mathbf{d}}_{\boldsymbol{\tau},p}) \end{array}\right) = \mathbf{0}. \tag{5.37}$$

The description of the iterative Active Set algorithm of index k in the context of a persistent contact is the following:
(i) Choose $(\mathbf{u}^{(0)}, \dot{\mathbf{u}}^{(0)}, \mathbf{\Gamma}^{(0)})$, $c_{\boldsymbol{\nu}} > 0$, $c_{\boldsymbol{\tau}} > 0$ and initialize $k = 0$.

(ii) if $d_{\boldsymbol{\nu}}^{\text{Leapfrog}} > 0$ set $\Gamma_{\boldsymbol{\nu},p}^{(k)} = 0$; $\mathbf{\Gamma}_{\boldsymbol{\tau},p}^{(k)} = 0$.

(iii) if $d_{\boldsymbol{\nu}}^{\text{Leapfrog}} \leq 0$ define the active and inactive sets:

$$\begin{aligned}
&\mathcal{A}_{\boldsymbol{\nu}}^{k+1} = \{p \in \mathcal{S} : \Gamma_{\boldsymbol{\nu},p}^{(k)} + c_{\boldsymbol{\nu}} \overset{\circ}{\mathbf{d}}{}_{\boldsymbol{\nu},p}^{(k)} < 0\},\\
&\mathcal{I}_{\boldsymbol{\nu}}^{k+1} = \mathcal{S} \setminus \mathcal{A}_{\boldsymbol{\nu}}^{k+1},\\
&\mathcal{A}_{\boldsymbol{\tau}}^{k+1} = \{p \in \mathcal{S} : \|\mathbf{\Gamma}_{\boldsymbol{\tau},p}^{(k)} + c_{\boldsymbol{\tau}} \overset{\circ}{\mathbf{d}}{}_{\boldsymbol{\tau},p}^{(k)}\| + \mu\Gamma_{\boldsymbol{\nu},p}^{(k)} \geq 0\},\\
&\mathcal{I}_{\boldsymbol{\tau}}^{k+1} = \mathcal{S} \setminus \mathcal{A}_{\boldsymbol{\tau}}^{k+1}.
\end{aligned}$$

(iv) Find $(\overset{\circ}{\mathbf{d}}{}^{(k+1)}, \mathbf{\Gamma}^{(k+1)})$ such that

$$\rho\ddot{\mathbf{u}}^{(k+1)} + A(\mathbf{u}^{(k+1)}, \dot{\mathbf{u}}^{(k+1)}) + \Gamma_{\boldsymbol{\nu}}^{(k+1)}\boldsymbol{\nu} + \mathbf{\Gamma}_{\boldsymbol{\tau}}^{(k+1)} = \mathbf{f} + \mathbf{g}, \tag{5.38}$$

$$\Gamma_{\boldsymbol{\nu},p}^{(k+1)} = 0, \quad \mathbf{\Gamma}_{\boldsymbol{\tau},p}^{(k+1)} = \mathbf{0} \quad \text{for all} \quad p \in \mathcal{I}_{\boldsymbol{\nu}}^{k+1}, \tag{5.39}$$

$$\overset{\circ}{d}{}_{\boldsymbol{\nu},p}^{(k+1)} = 0 \quad \text{for all} \quad p \in \mathcal{A}_{\boldsymbol{\nu}}^{k+1}, \tag{5.40}$$

$$\mathbf{\Gamma}_{\boldsymbol{\tau},p}^{(k+1)} = -\mu\Gamma_{\boldsymbol{\nu},p}^{(k+1)} \frac{\mathbf{\Gamma}_{\boldsymbol{\tau},p}^{(k)} + c_{\boldsymbol{\tau}} \overset{\circ}{\mathbf{d}}{}_{\boldsymbol{\tau},p}^{(k)}}{\|\mathbf{\Gamma}_{\boldsymbol{\tau},p}^{(k)} + c_{\boldsymbol{\tau}} \overset{\circ}{\mathbf{d}}{}_{\boldsymbol{\tau},p}^{(k)}\|} \quad \text{for all } p \in \mathcal{A}_{\boldsymbol{\tau}}^{k+1} \cap \mathcal{A}_{\boldsymbol{\nu}}^{k+1}, \tag{5.41}$$

$$\overset{\circ}{\mathbf{d}}{}_{\boldsymbol{\tau},p}^{(k+1)} + \frac{\overset{\circ}{\mathbf{d}}{}_{\boldsymbol{\tau},p}^{(k)}}{\Gamma_{\boldsymbol{\nu},p}^{(k)}} \Gamma_{\boldsymbol{\nu},p}^{(k+1)} = \overset{\circ}{\mathbf{d}}{}_{\boldsymbol{\tau},p}^{(k)} \quad \text{for all } p \in \mathcal{I}_{\boldsymbol{\tau}}^{k+1} \cap \mathcal{A}_{\boldsymbol{\nu}}^{k+1}. \tag{5.42}$$

(v) If $\|(\mathbf{u}^{(k+1)}, \mathbf{\Gamma}^{(k+1)}) - (\mathbf{u}^{(k)}, \mathbf{\Gamma}^{(k)})\| \leq \epsilon$, $\|\mathcal{R}(\mathbf{u}^{(k+1)}, \mathbf{\Gamma}^{(k+1)})\| \leq \epsilon$, $\mathcal{A}_{\boldsymbol{\nu}}^{k+1} = \mathcal{A}_{\boldsymbol{\nu}}^{k}$ and $\mathcal{A}_{\boldsymbol{\tau}}^{k+1} = \mathcal{A}_{\boldsymbol{\tau}}^{k}$ then stop, else return to (ii).

Remark 1. *One of the most interesting aspects of PDAS methods is that the resulting linear systems do not require the use of Lagrange multipliers and, therefore, become more simple to implement since the non-linear initial contact conditions are replaced at each iteration by the linear conditions* (5.39)*,* (5.40)*,* (5.41)*, and* (5.42) *which are Neumann, Dirichlet, and Robin-like conditions. Also, one of the specific features of the PDAS methods is to directly and strictly impose these conditions of contact computed by the iterative process of the semi-smooth Newton approach.*

6. Benchmark numerical simulations

In this section, we present numerical simulations always carried out with first-order finite elements, concerning space discretization. As for time discretization, time steps are suitably chosen as long as low-velocity impacts are considered.

6.1. Impact of a linear elastic ball against a foundation

We extend the problem to viscosity with the addition of a damping term:

$$W^v(\dot{\boldsymbol{\varepsilon}}) = \frac{\eta}{2}\text{tr}\,(\dot{\boldsymbol{\varepsilon}}^2) \tag{6.1}$$

where η is the damping factor. This representative benchmark problem describes the frictionless impact of a linear elastic ball against a foundation. The elastic ball is launched with an initial velocity $\mathbf{u}_1 = (0, -10)\,\mathrm{m/s}$ towards the foundation $\{(x_1, x_2) \in \mathbb{R}^2 : x_2 \leq 0\}$. The behavior of the material is described by a linear elastic constitutive law defined by the energy function

$$W^e(\boldsymbol{\varepsilon}) = \frac{E\kappa}{2(1+\kappa)(1-2\kappa)}(\mathrm{tr}\,\boldsymbol{\varepsilon})^2 + \frac{E}{2(1+\kappa)}\mathrm{tr}\,(\boldsymbol{\varepsilon}^2), \quad \forall \boldsymbol{\varepsilon} \in \mathbb{M}^2. \tag{6.2}$$

Here, E and κ are respectively the Young modulus and the Poisson ratio of the material and $\mathrm{tr}\,(\cdot)$ is the trace operator. Note that $\boldsymbol{\varepsilon} = \frac{1}{2}(\nabla \mathbf{u}^T + \nabla \mathbf{u})$ represents the linearized strain tensor within the framework of the theory of small strains ($\|\mathbf{u}\| \ll 1$ and $\|\nabla \mathbf{u}\| \ll 1$ in Ω). The physical framework is shown in Figure 2. The geometrical setting is

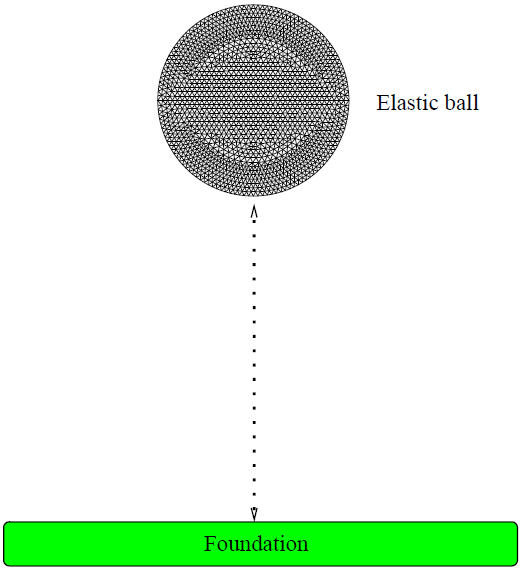

Figure 2: Discretization of the elastic ball in contact with a foundation.

given by

$$\begin{aligned}
\Omega &= \left\{(x_1, x_2) \in \mathbb{R}^2 : \ (x_1 - 100)^2 + (x_2 - 100)^2 \leq 100\right\}, \\
\partial_0\Omega &= \varnothing, \quad \partial_g\Omega = \varnothing, \\
\partial_c\Omega &= \left\{(x_1, x_2) \in \mathbb{R}^2 : \ (x_1 - 100)^2 + (x_2 - 100)^2 = 100\right\}.
\end{aligned}$$

The domain Ω represents the cross-section of the ball, assuming plane stress. We assume that volume forces do not act on the body during the process. For the discretization of the contact problem we use 7820 elastic nodes and 128 nodes for Lagrange multipliers. For the numerical experiments, we choose the following data set:

$$\begin{aligned}
&\rho = 1000\ \mathrm{kg/m^3}, \quad T = 2\,\mathrm{s}, \quad \Delta t = 0.001\,\mathrm{s}, \\
&\mathbf{u}_0 = (0,0)\,\mathrm{m}, \quad \mathbf{u}_1 = (0,-10)\,\mathrm{m/s}, \\
&E = 100\ \mathrm{GPa}, \quad \kappa = 0.35, \quad \mathbf{f} = (0,0)\,\mathrm{N/m^3}, \quad \mathbf{g} = (0,0)\ \mathrm{N/m^2}, \\
&g = 50\,\mathrm{m}, \quad \mu = 0,
\end{aligned}$$

where g is the initial gap. In Figure 3, the deformed ball sequence and contact stresses are shown before, during, and after impact. The interest of this representative example is to compare the numerical results of the Active Set

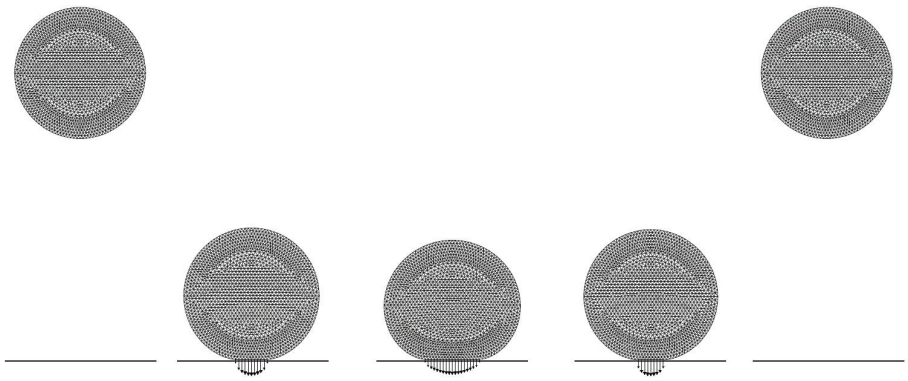

Figure 3: Sequence of deformed ball and contact stresses before, during, and after impact.

method with the results of other numerical methods obtained using certain classical methods. For this, we consider five existing methods:

– The classical quasi-Lagrangian method with the Signorini contact condition, see [42].
– The penalty method with a normal compliance condition of the form $\xi_{\boldsymbol{\nu}_n} = -r(u_{\boldsymbol{\nu}_n})_+$, with $r = 1000$.
– The specific penalization method developed by Hauret [16].
– The Equivalent Mass Matrix (EMM) method proposed by Khenous [70], which represents a specific distribution of the mass matrix without any inertia of the contact nodes. This method is characterized by relevant stability properties of the contact stress.
– Newton's adapted continuity method, developed by Ayyad and Barboteu [13], which is characterized by the application, after two steps, of the unilateral contact law and the condition of persistence during each time step.

In what follows, we analyze the methods with respect to the discrete energy evolution. Thus, the total discrete energy at time t_n is defined by the following formula:

$$E_n = \frac{1}{2}\int_\Omega \rho\|\dot{\mathbf{u}}_n^2\|\mathrm{d}x + \int_\Omega \boldsymbol{\sigma}_n^e : \boldsymbol{\varepsilon}(\mathbf{u}_n)\mathrm{d}x,$$

where $\boldsymbol{\varepsilon}$ denotes the infinitesimal strain tensor, and $\boldsymbol{\sigma}^e = \partial_{\boldsymbol{\varepsilon}} W^e(\boldsymbol{\varepsilon})$.

Figures (4) and (5) show the evolution of the total discrete energy of the system and the normal contact stress during the impact. After the impact, for the chosen time step and $t \geq 1.52$ s, the classical quasi-Lagrangian methods with Signorini's law (curve (⊖)) and the penalization method with normal compliance condition (curve (⊟)) do not conserve energy. The EMM method (curve ▼) greatly reduces power dissipation but fails to achieve exact conservation. The schemes developed by Ayyad and Barboteu [13] (curve (•)) and the specific penalty method developed by Hauret [16] (curve (■)) conserve energy after impact. However, for the penalized method of Hauret, there are energy fluctuations which disappear after the impact and for the scheme developed by Ayyad and Barboteu, we can note an increase in the normal contact stress. The Active Set method for persistent contact (shown by the curve (⧫)) allows energy to be conserved exactly without any fluctuation.

In order to overcome these difficulties, we consider the Active Set method with persistence and viscosity conditions, analyzing the behavior of discrete energy. From Figure 6, we can see that in the absence of viscosity ($\eta = 0$), this

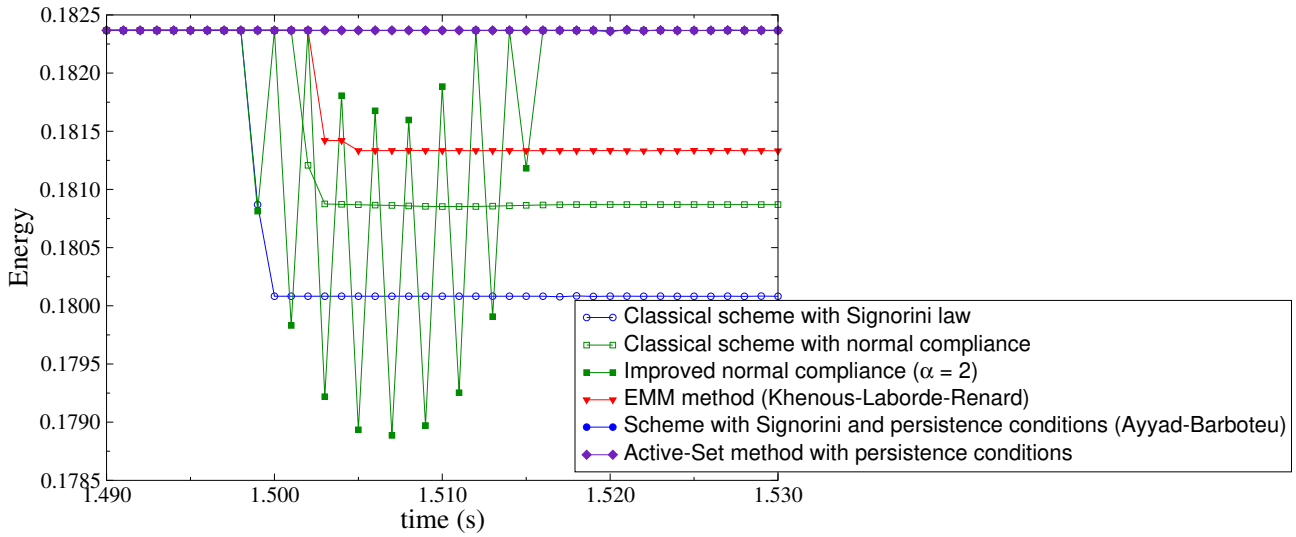

Figure 4: Discrete energy behavior of selected time integration schemes during impact.

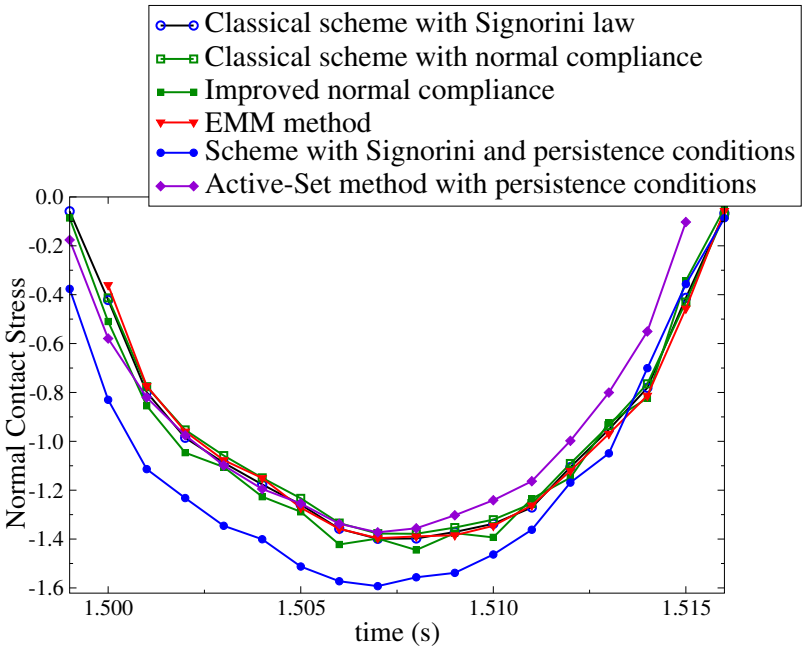

Figure 5: Normal contact stress of selected time integration schemes during impact.

method allows to obtain a better energy conservation. For $\eta > 0$, we see that the more the viscosity coefficient increases, the more the energy dissipates. Let us note that this dissipation does not results from a numerical artifact of the Active Set method, but it is a consequence of the hyper-viscoelastic model which one formulates. Indeed, we can notice that the Active Set method does not dissipate energy when we take a vanishing viscosity parameter.

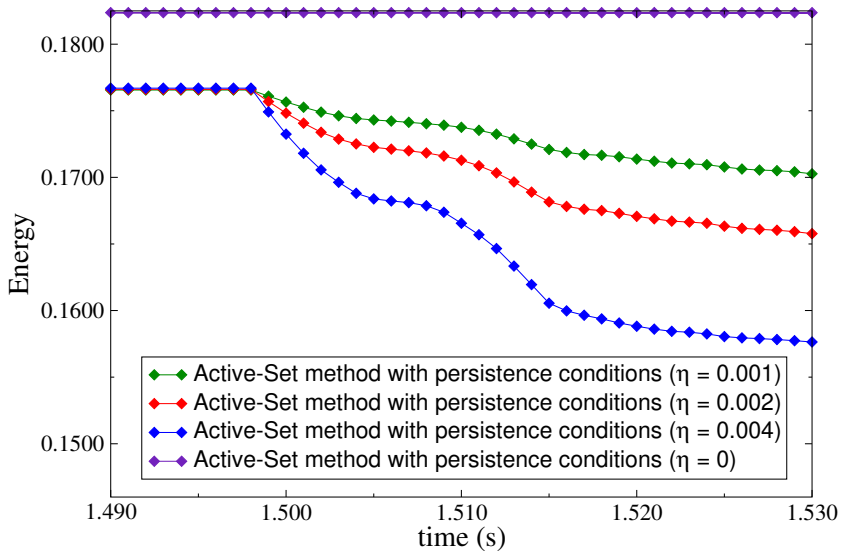

Figure 6: Discrete energy behavior for the Active Set method with persistence and viscosity (η) conditions.

6.2. Impact of a hyperelastic ring on a rigid foundation

The hyperelastic model is extended to viscosity with the addition of a damping term:

$$W^v(\dot{\mathbf{C}}) = \frac{\eta}{2}\mathrm{tr}\,(\dot{\mathbf{C}}^2). \tag{6.3}$$

The interest of this example is to give a validation of the hyper-viscoelastic frictional contact model proposed, compared to the results obtained by using Odgen's hyperelastic model. This non-trivial example, introduced by Laursen [7], concerns an academic problem of frictional impact of a hyper-viscoelastic ring against a foundation.

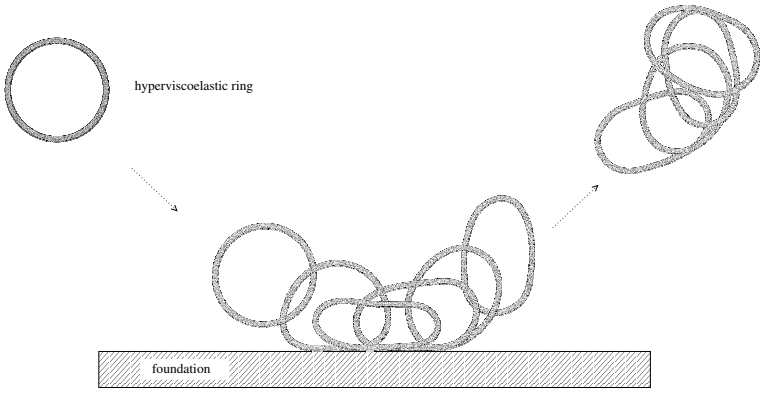

Figure 7: Sequence of the deformed hyper-viscoelastic ring before, during, and after impact.

For each hyperelastic model, we use the same viscous damping term given in (7.1). Details on the physical setting of the problem are given below:

$$\begin{aligned}
&\Omega = \left\{(x_1,x_2)\in\mathbb{R}^2 :\ 81 \le (x_1-100)^2+(x_2-100)^2 \le 100\right\},\\
&\partial_0\Omega = \varnothing, \qquad \partial_g\Omega = \left\{(x_1,x_2)\in\mathbb{R}^2 :\ (x_1-100)^2+(x_2-100)^2 = 81\right\},\\
&\partial_c\Omega = \left\{(x_1,x_2)\in\mathbb{R}^2 :\ (x_1-100)^2+(x_2-100)^2 = 100\right\}.
\end{aligned}$$

The domain Ω represents the cross-section of a three-dimensional deformable body under the assumption of plane stress. The ring is launched with an initial velocity at $45°$ with respect to the towards a foundation, as shown in Figure 7. The foundation is given by $\{(x_1, x_2) \in \mathbb{R}^2 : \ x_2 \leq 0\}$. For discretization, we use 1664 elastic nodes and 128 Lagrange multiplier nodes. The response of the compressible material is assumed to obey Ogden's constitutive law [71], characterized by the following energy density:

$$W(\mathbf{F}) = C_1(I_1 - 3) + C_2(I_2 - 3) + D(I_3 - 1) - (C_1 + 2C_2 + D)\ln I_3,$$

where the invariants I_1, I_2, and I_3 of $\mathbf{C} = \mathbf{F}^T\mathbf{F}$ are defined by

$$I_1(\mathbf{C}) = \mathrm{tr}(\mathbf{C}), \qquad I_2(\mathbf{C}) = \frac{(\mathrm{tr}(\mathbf{C}))^2 - \mathrm{tr}\,(\mathbf{C}^2)}{2}, \qquad I_3(\mathbf{C}) = \det(\mathbf{C}).$$

For numerical experiments, the data are:

$$\rho = 1000\,\mathrm{kg/m^3}, \quad T = 10\,\mathrm{s}, \quad \Delta t = \tfrac{1}{300}\,\mathrm{s},$$
$$\mathbf{u}_0 = (0,0)\,\mathrm{m}, \quad \mathbf{u}_1 = (10,-10)\,\mathrm{m/s}, \quad \mathbf{f} = (0,0)\,\mathrm{N/m^3}, \quad \mathbf{g} = (0,0)\ \mathrm{N/m^2},$$
$$C_1 = 0.5\,\mathrm{MPa}, \quad C_2 = 0.5 \cdot 10^{-2}\,\mathrm{MPa}, \quad D = 0.35\,\mathrm{MPa},$$
$$c_{\boldsymbol{\nu}} = 1000.$$

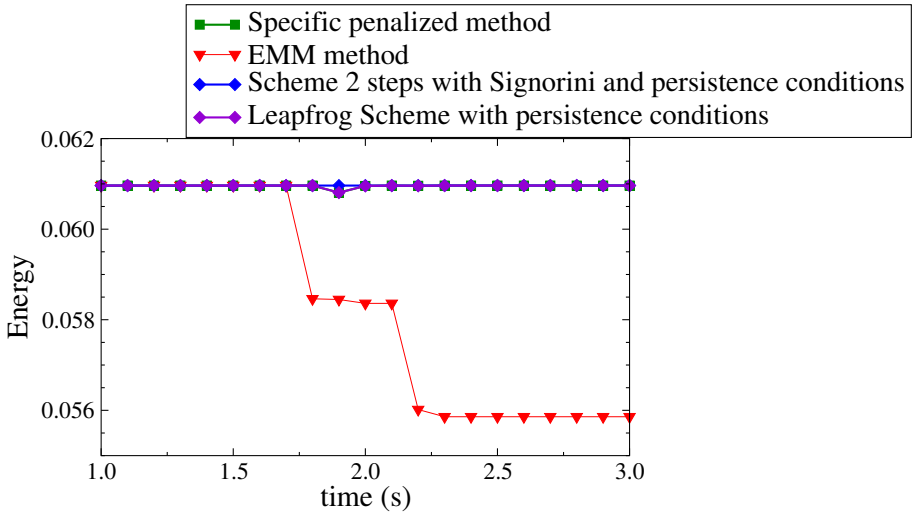

Figure 8: Discrete energy behavior of selected time integration schemes during impact.

In Figure 8, we observe the evolution of the total discrete energy of the frictionless dynamic system given by different time integration schemes. We find that the leapfrog scheme with persistent conditions, the 2-step scheme (Signorini and persistent condition) and the Hauret scheme (specific penalty) conserve energy unlike the EMM method (curve ▼) which dissipates energy.

Figure 9 presents the behavior of discrete energy using an Active Set scheme with persistent condition with frictionless viscosity. This method is characterized by a slightly dissipative behavior due to the viscosity. One can notice that the larger the viscosity parameter, the more the energy is dissipated. This is due to the hyper-viscoelastic model.

In Figure 10, we observe the behavior of discrete energy using an Active Set scheme with frictional contact. We see that for $\mu = 0$, this method allows to obtain an exact conservation of energy. When friction is taken into account

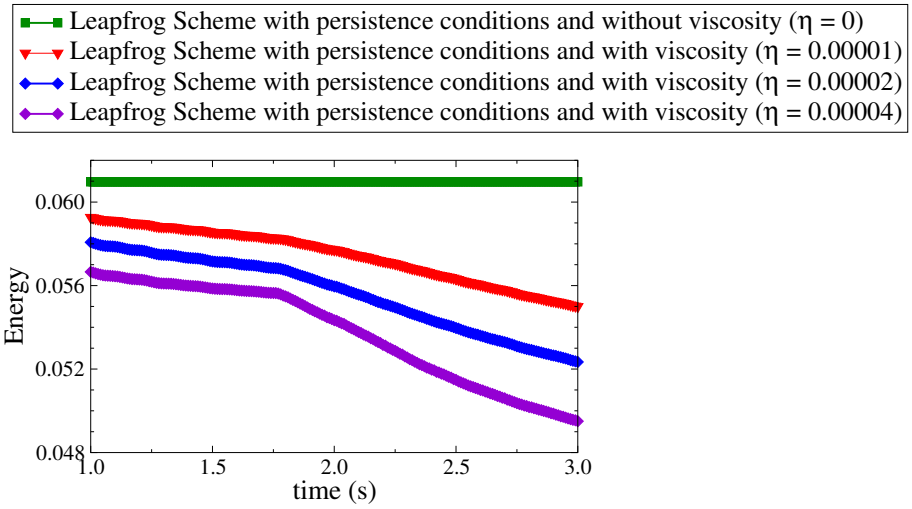

Figure 9: Discrete energy behavior with the PDAS–Leapfrog scheme with frictionless persistence and viscosity (η) conditions.

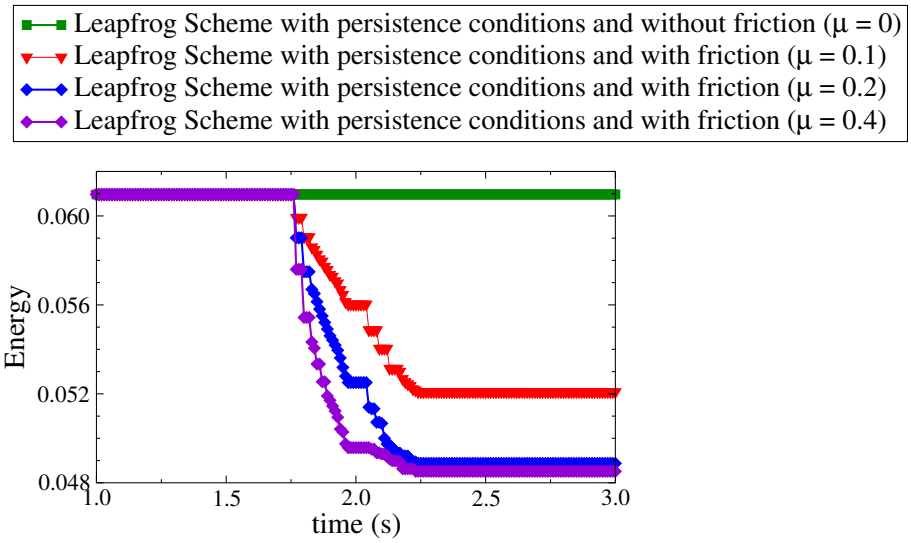

Figure 10: Discrete energy behavior with the PDAS–Leapfrog scheme with persistence and friction (μ) conditions without viscosity.

($\mu > 0$), this method presents a dissipation which increases with the friction coefficient, which clearly reflects the physical phenomenon of friction dissipation.

In Figure 11, the curves show the behavior of discrete energy using an Active Set scheme with viscosity and friction. For $(\mu, \eta) = (0, 0)$, we see an exact conservation of energy. On the other hand, for $\mu = 0.1$ and by considering $\eta \in \{0.0001, 0.0004\}$, we note that the dissipation of energy increases proportionally to the viscosity coefficient. This dissipation is physically acceptable.

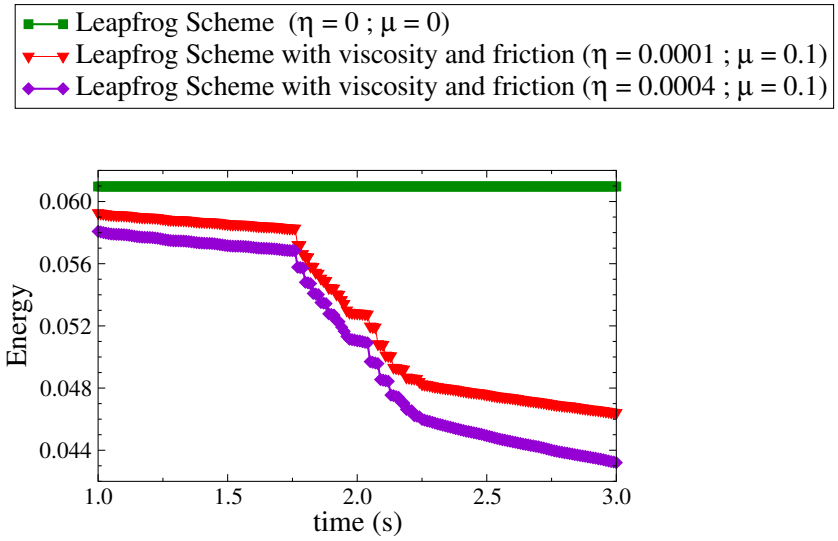

Figure 11: Discrete energy behavior with the PDAS–Leapfrog scheme with persistence, friction (μ) and viscosity (η) conditions.

7. Numerical simulation of a stent in contact with a soft tissue

As in previous simulations, the hyperelastic model is extended to viscosity with the addition of a damping term:

$$W^v(\dot{\mathbf{C}}) = \frac{\eta}{2}\mathrm{tr}\,(\dot{\mathbf{C}}^2). \tag{7.1}$$

The response of the compressible hyperelastic material is, again, described by Ogden's constitutive law [71],

$$W(\mathbf{F}) = C_1(I_1 - 3) + C_2(I_2 - 3) + D(I_3 - 1) - (C_1 + 2C_2 + D)\ln I_3.$$

The domain Ω represents a longitudinal section of a three-dimensional "stent–artery" system under the assumption of a plane stress. The stent is subjected to imposed displacements towards the walls of the artery, as illustrated in Figures 12 and 13. Concerning numerical experiments, the data are:

$$\begin{aligned}
&\rho = 1000\,\mathrm{kg/m^3}, \quad T = 1\,\mathrm{s}, \quad \Delta t = \tfrac{1}{50}\,\mathrm{s},\\
&C_1^{\text{artery}} = 0.5\,\mathrm{MPa}, \quad C_2^{\text{artery}} = 0.5\cdot 10^{-2}\,\mathrm{MPa}, \quad D^{\text{artery}} = 0.35\,\mathrm{MPa},\\
&C_1^{\text{stent}} = 2\cdot 10^{2}\,\mathrm{MPa}, \quad C_2^{\text{stent}} = 2\,\mathrm{MPa}, \quad D^{\text{stent}} = 140\,\mathrm{MPa},\\
&c_{\boldsymbol{\nu}} = 100000, \quad c_{\boldsymbol{\tau}} = 100.
\end{aligned}$$

For the discretization, we use 1137 elastic nodes. The simulation CPU time for a deformed "stent-artery" configuration (see Figure 14) is of the order of 55 seconds.

We can notice in Figure 14 that the stent adheres to the wall of the artery according to the displacement imposed. In what follows, we will study the behavior of the difference in discrete energy between the times t_{i+1} and t_i for the PDAS–Leapfrog scheme as indicated below:

$$\Delta E = E_{i+1} - E_i = -\Delta t \int_{\partial_c\Omega} (\Gamma_{\boldsymbol{\nu}_{i+\frac{1}{2}}}\,\delta\mathring{d}_{\boldsymbol{\nu}_{i+\frac{1}{2}}} + \boldsymbol{\Gamma}_{\boldsymbol{\tau}_{i+\frac{1}{2}}}\cdot\delta\mathring{\mathbf{d}}_{\boldsymbol{\tau}_{i+\frac{1}{2}}})\;\mathrm{d}a - D_{i+\frac{1}{2}}. \tag{7.2}$$

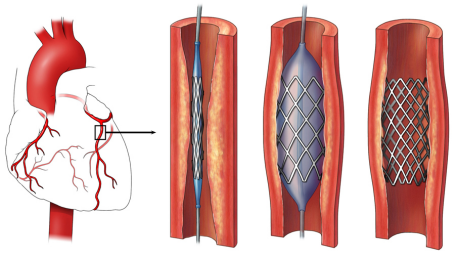

Figure 12: Stainless-steel stent in an arterial tissue. Source: National Heart, Lung, and Blood Institute; National Institutes of Health; U.S. Department of Health and Human Services.

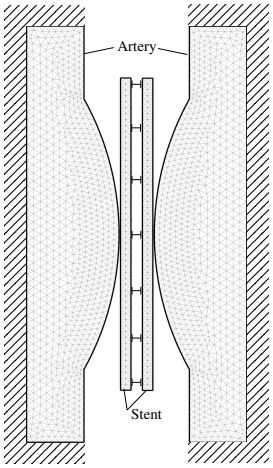

Figure 13: Configuration of the meshes of the stent-artery assembly in the initial state.

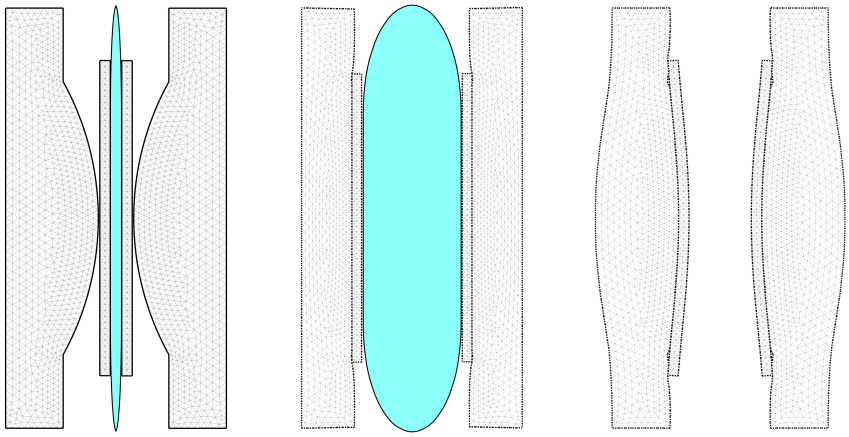

Figure 14: Distorted meshes of the artery-stent assembly.

In Figure 15, when friction is absent, we observe that without viscosity ($\eta = 0$), the difference in discrete energy is practically zero, which indicates that this method allows energy conservation. In the presence of viscosity, we note that the higher the value of η, the greater the dissipation (ΔE is negative). This confirms what we observed in the continuous and discrete case.

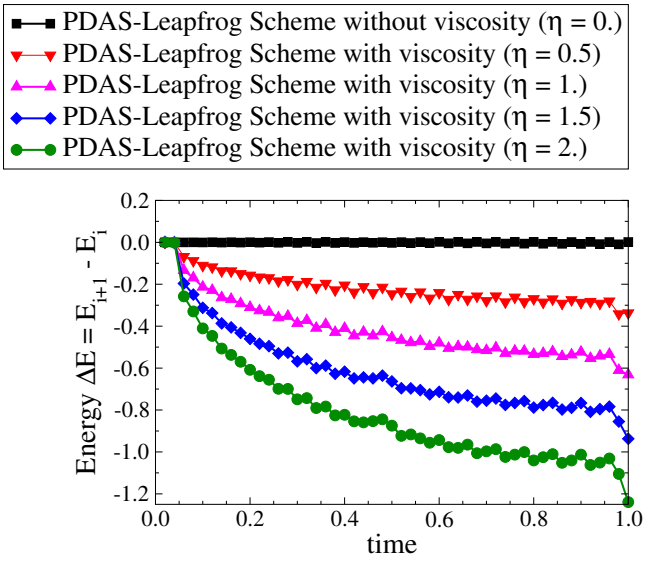

Figure 15: Behavior of the discrete energy difference between the times t_{i+1} and t_i for the PDAS–Leapfrog scheme with contact conditions, without friction and with viscosity (η).

In Figure 16, in the presence of viscosity ($\eta = 1$), and in the absence of friction, energy is dissipated. When friction

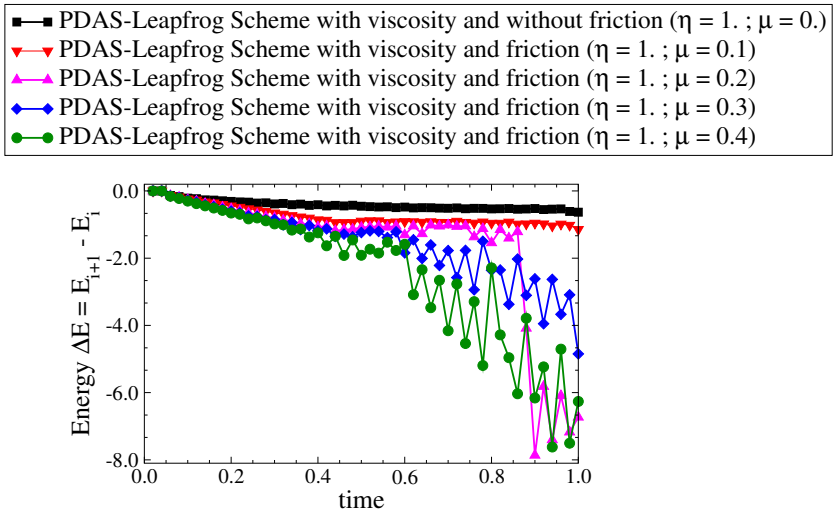

Figure 16: Discrete energy difference between the times t_{i+1} and t_i for the PDAS–Leapfrog scheme with conditions of contact, friction (μ), and viscosity (η).

is taken into account, we notice that this dissipation increases according to the coefficient of friction μ. We can also notice that the more μ increases, the more relevant are fluctuations, but ΔE always remains negative.

8. Conclusion and perspectives

In this work, we have addressed a problem in hyper-viscoelastic dynamics with persistence conditions, both with and without friction. From the computational viewpoint, a novel numerical method is presented: the Active Set

method based on an iterative Newton semi-smooth scheme with persistence conditions. A comparative study is then conducted between the proposed Active Set method and other methods, in terms of energy behavior. Numerical tests have shown that the implemented strategy exhibits good energy conservation properties during impact without friction and without viscosity, and that it dissipates energy in the cases with friction and viscosity, as expected.
Many open problems can be considered as future perspectives. For instance, it would be interesting to study other constitutive laws such as perfectly plastic or visco-plastic materials in the context of hyperelasticity and to propose an analysis of the energy balance of these dissipative systems [72]. These laws can be associated with different conditions of contact and friction, thus posing new challenges, in particular the extension of Semi-Smooth Newton and PDAS methods. Another important perspective concerns numerical simulations in a three-dimensional framework, in order to make predictions of real-life scenarios in line with soft tissue biomechanical experimental systems.

References

[1] T. Hu and J.P. Desai. Characterization of soft-tissue material properties: large deformation analysis. In *Medical Simulation*, volume 3078, pages 28–37, 2004.

[2] D.R. Nolan, A.L. Gower, M. Destrade, R.W. Ogden, and J.P. McGarry. A robust anisotropic hyperelastic formulation for the modelling of soft tissue. *Journal of the Mechanical Behavior of Biomedical Materials*, 39:48–60, 2014.

[3] D.P. Pioletti and L.R. Rakotomanana. Non-linear viscoelastic laws for soft biological tissues. *Eur. J. Mech. A/Solids*, 19:749–759, 2000.

[4] G.Z. Voyiadjis and A. Samadi-Dooki. Hyperelastic modeling of the human brain tissue: Effects of no-slip boundary condition and compressibility on the uniaxial deformation. *Journal of the Mechanical Behavior of Biomedical Materials*, 83:63–78, 2018.

[5] K. Upadhyay, G. Subhash, and D. Spearot. Visco-hyperelastic constitutive modeling of strain rate sensitive soft materials. *Journal of the Mechanics and Physics of Solids*, 135:103777, 2020.

[6] G. Chagnon, M. Rebouah, and D. Favier. Hyperelastic energy densities for soft biological tissues: A review. *Journal of Elasticity, Springer Verlag*, 120:129–160, 2015.

[7] T.A. Laursen. *Computational contact and impact mechanics: fundamentals of modeling interfacial phenomena in nonlinear finite element analysis*. Springer Science & Business Media, 2003.

[8] P. Wriggers and G. Zavarise. Computational contact mechanics. *Encyclopedia of Computational Mechanics*, 2004.

[9] V. Acary and B. Brogliato. *Numerical methods for nonsmooth dynamical systems: applications in mechanics and electronics*. Springer Science & Business Media, 2008.

[10] B. Brogliato. *Impacts in Mechanical Systems: Analysis and Modelling*. Springer Science & Business Media, 2000.

[11] M. Sofonea and A. Matei. *Mathematical models in contact mechanics*, volume 398. Cambridge University Press, 2012.

[12] T.A. Laursen and V. Chawla. Design of energy conserving algorithms for frictionless dynamic contact problems. *International Journal for Numerical Methods in Engineering*, 40(5):863–886, 1997.

[13] Y. Ayyad and M. Barboteu. Formulation and analysis of two energy-consistent methods for nonlinear elastodynamic frictional contact problems. *Journal of computational and applied mathematics*, 228(1):254–269, 2009.

[14] O. Gonzalez. Exact energy and momentum conserving algorithms for general models in non linear elasticity. *Computer Methods in Applied Mechanics and Engineering*, 190:1763–1783, 2000.

[15] T.A. Laursen and G. Love. Improved implicit integrators for transient impact problems: dynamic frictional dissipation within an admissible conserving framework. *Computer Methods in Applied Mechanics and Engineering*, 192:2223–2248, 2003.

[16] P. Hauret and P. Le Tallec. Energy-controlling time integration methods for nonlinear elastodynamics and low-velocity impact. *Computer Methods in Applied Mechanics and Engineering*, 195(37-40):4890–4916, 2006.

[17] M. Barboteu, D. Danan, and M. Sofonea. A hyperelastic dynamic frictional contact model with energy-consistent properties. In *Advances in Variational and Hemivariational Inequalities*, pages 249–275. Springer, 2015.

[18] L. Noels, L. Stainier, and J. P. Ponthot. An energy momentum conserving algorithm for non-linear hypoelastic constitutive models. *International Journal for Numerical Methods in Engineering*, 59(1):83–114, 2004.

[19] S. Conde Martín, J.C. García Orden, and I. Romero. Energy-consistent time integration for nonlinear viscoelasticity. *Computational Mechanics*, 54(2):473–488, 2014.

[20] P. Betsch, A. Janz, and C. Hesch. A mixed variational framework for the design of energy–momentum schemes inspired by the structure of polyconvex stored energy functions. *Computer Methods in Applied Mechanics and Engineering*, 335:660–696, 2018.

[21] M. Franke, D.K. Klein, O. Weeger, and P. Betsch. Advanced discretization techniques for hyperelastic physics-augmented neural networks. *Computer Methods in Applied Mechanics and Engineering*, 416:116333, 2023.

[22] J.J. Moreau. Numerical aspects of the sweeping process. *Computer Methods in Applied Mechanics and Engineering*, 177(3-4):329–349, 1999.

[23] J. Simo and N. Tarnow. The discrete energy-momentum method. part i: Conserving algorithms for nonlinear elastodynamics. *Zeitschrift für Angewandte Mathematik und Physik*, 43:757–793, 1992.

[24] F. Armero and I. Romero. On the formulation of high-frequency dissipative time-stepping algorithms for nonlinear dynamics. part ii: second-order methods. *Computer Methods in Applied Mechanics and Engineering*, 190:6783–6824, 2001.

[25] T.A. Laursen and V. Chawla. Design of energy-conserving algorithms for frictionless dynamic contact problems. *International Journal for Numerical Methods in Engineering*, 40:863–886, 1997.

[26] F. Armero and E. Petocz. Formulation and analysis of conserving algorithms for frictionless dynamic contact/impact problems. *Computer Methods in Applied Mechanics and Engineering*, 158:269–300, 1998.

[27] V. Acary. Projected event-capturing time-stepping schemes for nonsmooth mechanical systems with unilateral contact and coulomb's friction. *Computer Methods in Applied Mechanics and Engineering*, 256:224–250, 2013.

[28] V. Acary. Energy conservation and dissipation properties of time-integration methods for nonsmooth elastodynamics with contact. *ZAMM-Journal of Applied Mathematics and Mechanics/Zeitschrift für Angewandte Mathematik und Mechanik*, 96(5):585–603, 2016.

[29] P. Betsch and C. Hesch. Energy-momentum conserving schemes for frictionless dynamic contact problems. In Peter Wriggers and Udo Nackenhorst, editors, *IUTAM Symposium on Computational Methods in Contact Mechanics*, pages 77–96, Dordrecht, 2007. Springer Netherlands.

[30] C. Hesch and P. Betsch. Transient 3d contact problems–NTS method: mixed methods and conserving integration. *Computational Mechanics*, 48:437–449, 2011.

[31] C. Hesch and P. Betsch. Transient three-dimensional contact problems: mortar method. mixed methods and conserving integration. *Computational Mechanics*, 48:461–475, 2011.

[32] C. Hesch and P. Betsch. A mortar method for energy-momentum conserving schemes in frictionless dynamic contact problems. *International Journal for Numerical Methods in Engineering*, 77(10):1468–1500, 2009.

[33] C. Agelet de Saracibar and D. Di Capua. Conserving algorithms for frictionless and full stick friction dynamic contact problems using the direct elimination method. *International Journal for Numerical Methods in Engineering*, 113(6):910–937, 2018.

[34] M.A. Puso. An energy and momentum conserving method for rigid–flexible body dynamics. *International Journal for Numerical Methods in Engineering*, 53(6):1393–1414, 2002.

[35] M.A. Puso, T.A. Laursen, and J. Solberg. A segment-to-segment mortar contact method for quadratic elements and large deformations. *Computer methods in applied mechanics and engineering*, 197(6-8):555–566, 2008.

[36] G. Haikal and K.D. Hjelmstad. A finite element formulation of non-smooth contact based on oriented volumes for quadrilateral and hexahedral elements. *Computer Methods in Applied Mechanics and Engineering*, 196(45-48):4690–4711, 2007.

[37] Y. Ayyad, M Barboteu, and J.R. Fernández. A frictionless viscoelastodynamic contact problem with energy consistent properties: Numerical analysis and computational aspects. *Computer Methods in Applied Mechanics and Engineering*, 198(5-8):669–679, 2009.

[38] N. Kikuchi and J.T. Oden. *Contact Problems in Elasticity: A Study of Variational Inequalities and Finite Element Methods*. SIAM Studies in Applied Mathematics, vol. 8, Philadelphia, 1988.

[39] J.T. Oden and S.J. Kim. Interior penalty methods for finite element approximations of the Signorini problem in elastostatics. *Computers and Mathematics with Applications*, 8(1):35–56, 1986.

[40] J.A.C. Martins and J.T. Oden. Existence and uniqueness results for dynamic contact problems with nonlinear normal and friction interface laws. *Nonlinear Analysis – Theory, Methods & Applications*, 11:407–428, 1987.

[41] M. Barboteu, F. Bonaldi, D. Danan, and S. El Hadri. An Improved Normal Compliance method for dynamic hyperelastic problems with energy conservation property. *Commun. Nonlinear Sci. Numer. Simul.*, 123:107296, 2023.

[42] P. Alart and A. Curnier. A mixed formulation for frictional contact problems prone to newton like solution methods. *Computer Methods in Applied Mechanics and Engineering*, 92(3):353–375, 1991.

[43] G. de Saxcé and Z-Q. Feng. New inequality and functional for contact with friction: the implicit standard material approach. *Journal of Structural Mechanics*, 19(3):301–325, 1991.

[44] S. Dumont. On enhanced descent algorithms for solving frictional multicontact problems: application to the discrete element method. *International Journal for Numerical Methods in Engineering*, 93(11):1170–1190, 2013.

[45] M. Raous, P. Chabrand, and F. Lebon. Numerical methods for solving unilateral contact problem with friction. *Journal of Theoretical and Applied Mechanics*, 7:111–128, 1988.

[46] P. Joli and Z.-Q. Feng. Uzawa and newton algorithms to solve frictional contact problems within the bi-potential framework. *International Journal for Numerical Methods in Engineering*, 73(3):317–330, 2008.

[47] F. Chouly. An adaptation of Nitsche's method to the tresca friction problem. *Journal of Mathematical Analysis and Applications*, 411(1):329–339, 2014.

[48] F. Chouly, P. Hild, and Y. Renard. A Nitsche finite element method for dynamic contact: 1. space semi-discretization and time-marching schemes. *ESAIM: Mathematical Modelling and Numerical Analysis*, 49(2):481–502, 2015.

[49] F. Chouly, M. Fabre, P. Hild, R. Mlika, J. Pousin, and Y. Renard. An overview of recent results on Nitsche's method for contact problems. *Geometrically unfitted finite element methods and applications*, pages 93–141, 2017.

[50] F. Chouly, P. Hild, and Y. Renard. *Finite Element Approximation of Contact and Friction in Elasticity*, volume 48 of *Advances in Mechanics and Mathematics*. Springer International Publishing, 2023.

[51] M. Hintermüller, K. Ito, and K. Kunisch. The primal-dual active set strategy as a semismooth Newton method. *SIAM Journal on Optimization*, 13(3):865–888, 2002.

[52] M. Hintermüller, V. A Kovtunenko, and K. Kunisch. *Semismooth Newton methods for a class of unilaterally constrained variational problems*. Universität Graz/Technische Universität Graz. SFB F003-Optimierung und Kontrolle, 2003.

[53] S. Hüeber and B. Wohlmuth. A primal–dual active set strategy for non-linear multibody contact problems. *Computer Methods in Applied Mechanics and Engineering*, 194(27-29):3147–3166, 2005.

[54] S. Hüeber, G. Stadler, and B. Wohlmuth. A primal-dual active set algorithm for three-dimensional contact problems with coulomb friction. *SIAM Journal on Scientific Computing*, 30(2):572–596, 2008.

[55] K. Kunisch and G. Stadler. Generalized Newton methods for the 2d-Signorini contact problem with friction in function space. *ESAIM: Mathematical Modelling and Numerical Analysis*, 39(4):827–854, 2005.

[56] S. Abide, M. Barboteu, and D. Danan. Analysis of two active set type methods to solve unilateral contact problems. *Applied Mathematics and Computation*, 284:286–307, 2016.

[57] S. Abide, M. Barboteu, S. Cherkaoui, D. Danan, and S. Dumont. Inexact primal–dual active set method for solving elastodynamic frictional contact problems. *Computers and Mathematics with Applications*, 82:36–59, 2021.

[58] S. Abide, M. Barboteu, S. Cherkaoui, D. Danan, and S. Dumont. A semi-smooth newton and primal-dual active set method for non-smooth contact dynamics. *Computers and Mathematics with Applications*, 387:114153, 2021.

[59] P.G. Ciarlet. *Mathematical Elasticity: Volume I: three-dimensional elasticity*. North-Holland, 1988.

[60] P. Le Tallec. Numerical methods for nonlinear three-dimensional elasticity, in Handbook of Numerical Analysis, 1994.

[61] J.J. Moreau. Unilateral contact and dry friction in finite freedom dynamics. In *Nonsmooth mechanics and Applications*, pages 1–82. Springer, 1988.

[62] Y. Desplanques. Amontons-Coulomb friction laws, a review of the original manuscript. *SAE International Journal of Materials and Manufacturing*, 8(1):98–103, 2015.

[63] M. Jean. The non-smooth contact dynamics method. *Computer Methods in Applied Mechanics and Engineering*, 177(3-4):235–257, 1999.

[64] G. Pietrzak. *Continuum mechanics modelling and augmented Lagrangian formulation of large deformation frictional contact problems*. PhD thesis, Lausanne, 1997.

[65] G. Pietrzak and A. Curnier. Large deformation frictional contact mechanics: continuum formulation and augmented lagrangian treatment. *Computer Methods in Applied Mechanics and Engineering*, 177(3-4):351–381, 1999.

[66] A. Curnier. *Méthodes numériques en mécanique des solides*. Presses polytechniques et universitaires romandes, 2001.

[67] D.P. Pioletti, L.R. Rakotomanana, J.F. Benvenuti, and P.F. Leyvraz. Viscoelastic constitutive law in large deformations: application to human knee ligaments and tendons. *J. Biomech.*, 31(8):753–7, 1998.

[68] H.M. Hilber, T. Hughes, and R.L. Taylor. Improved numerical disspation for time integration algorithms in structural dynamics. *Earthquake Engineering and Structural Dynamics*, 5:283–292, 1977.

[69] C. Hesch and P. Betsch. Transient three-dimensional domain decomposition problems: Frame-indifferent mortar constraints and conserving integration. *International Journal for Numerical Methods in Engineering*, 82(3):329–358, 2010.

[70] H.B. Khenous, P. Laborde, and Y. Renard. On the discretization of contact problems in elastodynamics. In *Analysis and simulation of contact problems*, pages 31–38. Springer, 2006.

[71] P.G. Ciarlet and G. Geymonat. Sur les lois de comportement en élasticité non-linéaire compressible. *C. R. Acad. Sci.*, 295:423–426, 1982.

[72] G. Kluth. *Analyse mathématique et numérique de systèmes hyperélastiques et introduction de la plasticité*. PhD thesis, Laboratoire Jacques Louis Lions de l'Université Pierre et Marie Curie, Paris VI, 2008.